NASA TN D-4434

AN ANALYTICAL PROCEDURE FOR PREDICTING THE TWO-DIMENSIONAL IMPACT DYNAMICS OF SPACECRAFT LANDING GEAR

By James T. Howlett

Langley Research Center
Langley Station, Hampton, Va.

NATIONAL AERONAUTICS AND SPACE ADMINISTRATION

For sale by the Clearinghouse for Federal Scientific and Technical Information
Springfield, Virginia 22151 – CFSTI price $3.00

AN ANALYTICAL PROCEDURE FOR PREDICTING THE TWO-DIMENSIONAL IMPACT DYNAMICS OF SPACECRAFT LANDING GEAR

By James T. Howlett
Langley Research Center

SUMMARY

This paper presents a method for analyzing the dynamic behavior of two-dimensional impacting struts and trusses of the type presently used in the construction of landing gear for lunar landing vehicles. The struts and trusses may contain shock absorbers. The method uses lumped masses to represent the system, and two-dimensional motion is assumed. The equations of motion are numerically integrated to obtain response time histories of each of the mass points, and to allow detailed analysis of the dynamic behavior of the system. Application of the method to a particular strut and truss indicates that axial elasticity is much more important than lateral elasticity in the dynamic behavior. The present limitation of the method is the large amount of computer time required for problems in which the time period of interest is large compared with the period of the highest natural frequency of the system.

INTRODUCTION

Current concepts for space vehicles for soft landing on lunar and planetary surfaces include landing gears consisting of legs which are trusses constructed of tubular struts. The truss members may contain some type of shock absorber. In order to assure proper functioning of such landing gears, it is essential to understand the dynamic behavior upon impact with a landing surface. Especially important are the buckling behavior of the landing gear and the effects of landing-gear elasticity on the landing dynamics of the vehicle.

Previous analyses of landing dynamics (for example, refs. 1 and 2) have included axial but not lateral vibrations of the landing gear. Drop tests of a model of an early version of the lunar module have shown that the landing gear undergoes lateral vibrations during impact. The effect of lateral vibrations was not clearly understood. Accordingly, the study reported herein was carried out. It consists of a mathematical analysis of the dynamic behavior of impacting trusses containing shock absorbers with

lateral oscillations included as a possible deformation. The analysis, which is restricted to two-dimensional motion, represents the truss by a finite-element lumped-mass system, uses Euler's method of numerical integration to obtain response time histories of each mass point, and thus allows detailed examination of the dynamic behavior of the truss. The analysis is applied to a specific strut and truss configuration to serve as an example.

SYMBOLS

d_1, d_2	distances between vehicle center of mass and masses k_1 and $k_1 + 1$
EA	axial stiffness
EI	flexural stiffness
F	force
I	moment of inertia
$k = \sqrt{\frac{\lvert P \rvert}{EI}}$	
l	length of beam-column element
m	mass
M	moment
P	axial load
t	time
X,Y	axes of inertial coordinate system
x,y	distance along axes
α	slope in inertial coordinate system
δ	total shortening of beam-column element
δ_1	shortening due to bending defined by equation (14)

δ_2 shortening due to compression defined by equation (26)

$\eta(\xi)$ lateral deflection in local coordinate system

$\eta_l = \eta(l)$

θ slope of free end of beam-column element in local coordinate system

ξ,η axes of local coordinate system

ρ radius of gyration of cross section

Subscripts:

c_1 mass on main strut to which secondary strut is joined

c_2 mass at end of secondary strut which attaches to main strut

cm vehicle center of mass

j jth mass point

j,j-1 jth mass point referred to first local coordinate system

j,j+1 jth mass point referred to second local coordinate system

k_1 mass point at vehicle end of main strut

k_1+1 mass point at vehicle end of secondary strut

X,Y,α components of forces

t total

e external

Matrix notations:

$\{\}$ column matrix

$[\,]$ square matrix

Dots over a symbol denote differentiation with respect to time. Primes denote differentiation in the local coordinate systems with respect to ξ. A bar over a symbol denotes a nondimensional quantity.

ANALYSIS

The basic method of analysis is first developed for a strut. In a later section the method is generalized to include a truss containing shock absorbers.

A strut is represented by a number of point masses connected by massless beam-column elements which may undergo both axial and lateral deformations. (See fig. 1.) Each of these elements is uniform, but the length and stiffness parameters may differ from one element to the next. Only two-dimensional motion is allowed.

Coordinate Systems

As shown in figure 1, three different types of coordinate systems are used in the analysis. The axes of the inertial coordinate system are denoted by X and Y. In addition to the inertial coordinate system, there are two local coordinate systems associated with each mass point. The local coordinate systems are attached to the strut and move with it. The axes of the first local coordinate system associated with the jth mass are denoted by $\xi_{j,j-1}$ and $\eta_{j,j-1}$. The origin of the first local coordinate system is located at mass $j - 1$. The $\xi_{j,j-1}$-axis is tangent to the strut at mass $j - 1$ and positive in the direction of the jth mass. The positive direction of the $\eta_{j,j-1}$-axis is 90^o counterclockwise from the positive $\xi_{j,j-1}$-axis.

The axes of the second local coordinate system associated with the jth mass are denoted by $\xi_{j,j+1}$ and $\eta_{j,j+1}$. The origin of the second local coordinate system is located at mass $j + 1$. The $\xi_{j,j+1}$-axis is tangent to the strut at mass $j + 1$ and positive in the direction of the jth mass. The positive direction of the $\eta_{j,j+1}$-axis is 90^o counterclockwise from the positive $\xi_{j,j+1}$-axis.

Equations of Motion

Newton's equations of motion for the system take the following form for $j = 1, 2, \ldots, k_1$:

$$m_j\ddot{x}_j = F_{X_{j,j-1}} + F_{X_{j,j+1}} + F_{e,X_j} \tag{1a}$$

$$m_j\ddot{y}_j = F_{Y_{j,j-1}} + F_{Y_{j,j+1}} + F_{e,Y_j} \tag{1b}$$

$$I_j\ddot{\alpha}_j = F_{\alpha j,j-1} + F_{\alpha j,j+1} \tag{1c}$$

where

m_j jth mass

I_j moment of inertia associated with jth mass

$F_{X_{j,j-1}}, F_{Y_{j,j-1}}, F_{\alpha_{j,j-1}}$ forces and the moment acting on jth mass from beam column j,j-1

$F_{X_{j,j+1}}, F_{Y_{j,j+1}}, F_{\alpha_{j,j+1}}$ forces and the moment acting on jth mass from beam column j,j+1

F_{e,X_j}, F_{e,Y_j} components of external forces acting on jth mass

Quantities with nonpositive subscripts or subscripts greater than k_1 do not appear. The procedure for computing the quantities $F_{X_{j,j-1}}$, $F_{Y_{j,j-1}}$, $F_{\alpha_{j,j-1}}$, $F_{X_{j,j+1}}$, $F_{Y_{j,j+1}}$, and $F_{\alpha_{j,j+1}}$ is given in the following section. Since the equations which are used to compute these quantities are nonlinear, the values are computed numerically for each time step. Once the values are determined, Euler's method is used to integrate equations (1) one time step with the assumption that $F_{X_{j,j-1}}$, $F_{Y_{j,j-1}}$, $F_{\alpha_{j,j-1}}$, $F_{X_{j,j+1}}$, $F_{Y_{j,j+1}}$, and $F_{\alpha_{j,j+1}}$ remain constant during the interval.

Force-Displacement Equations

To determine the quantities $F_{X_{j,j-1}}$, $F_{Y_{j,j-1}}$, and $F_{\alpha_{j,j-1}}$, the elastic forces exerted on the jth mass by the beam column connecting masses $j - 1$ and j must be determined. These forces can be determined by standard procedures. Classical beam-column theory gives equations relating the forces and displacements of the two ends of the beam column. These equations are more conveniently expressed in the first local coordinate system. The position of and slope at the jth mass in the first local coordinate system are given by the following formulas (fig. 1):

$$\xi_{j,j-1} = (x_j - x_{j-1})\cos \alpha_{j-1} + (y_j - y_{j-1})\sin \alpha_{j-1} \tag{2a}$$

$$\eta_{j,j-1} = -(x_j - x_{j-1})\sin \alpha_{j-1} + (y_j - y_{j-1})\cos \alpha_{j-1} \tag{2b}$$

$$\theta_{j,j-1} = \alpha_j - \alpha_{j-1} \tag{2c}$$

Also define

$$\delta_{j,j-1} = l_{j,j-1} - \xi_{j,j-1} \tag{3}$$

where $l_{j,j-1}$ is the undeformed length of the beam column connecting masses $j - 1$ and j. The quantity $\delta_{j,j-1}$ is called the total shortening of the beam column connecting masses $j - 1$ and j.

For notational convenience, the subscripts are dropped with the understanding that the quantities are in the first local coordinate system. Note that in the first local coordinate system, the beam column connecting masses $j - 1$ and j may be viewed as a cantilevered beam column (isolated section of fig. 1). In general, three types of loads may be needed at the free end of this element to hold it statically in its instantaneous deformed configuration: a lateral force F, an applied moment M, and an end load P. The following procedure is a well-known method of relating the forces to the displacements.

The equation for the lateral deflection of the cantilevered beam column shown in the isolated section of figure 1 is

$$\frac{d^2\eta(\xi)}{d\xi^2} = \frac{M_t}{EI} \tag{4}$$

where

$\eta(\xi)$ lateral deflection

EI flexural stiffness

M_t total bending moment

Note that

$$\eta(l) = \eta_l = \eta_{j,j-1} \tag{5}$$

where $\eta_{j,j-1}$ is given by equation (2b).

The boundary conditions are

$$\eta(0) = 0 \tag{6a}$$

$$\frac{d\eta(0)}{d\xi} = 0 \tag{6b}$$

Two different cases may arise: for case 1, $P = 0$; for case 2, $P \neq 0$.

Case 1; $P = 0$.- In this case, equation (4) becomes

$$\frac{d^2\eta(\xi)}{d\xi^2} = \frac{1}{EI}\left[M + F(l - \xi)\right] \tag{7}$$

The solution of equation (7) subject to boundary conditions (6) is

$$\eta(\xi) = \frac{1}{EI}\left[(M + Fl)\frac{\xi^2}{2} - \frac{F\xi^3}{6}\right] \tag{8}$$

At the free end

$$\eta_l = \eta(l) = \frac{1}{EI}\left[(M + Fl)\frac{l^2}{2} - \frac{Fl^3}{6}\right] \tag{9a}$$

$$\theta = \eta'(l) = \frac{1}{EI}\left[(M + Fl)l - \frac{Fl^2}{2}\right] \tag{9b}$$

or in matrix form

$$\begin{Bmatrix} \eta_l \\ \theta \end{Bmatrix} = \frac{1}{EI}\begin{bmatrix} \frac{l^3}{3} & \frac{l^2}{2} \\ \frac{l^2}{2} & l \end{bmatrix}\begin{Bmatrix} F \\ M \end{Bmatrix} \tag{10}$$

Inverting equation (10) gives the relationship between the forces and displacements

$$\begin{Bmatrix} F \\ M \end{Bmatrix} = \frac{12EI}{l^4}\begin{bmatrix} l & -\frac{l^2}{2} \\ -\frac{l^2}{2} & \frac{l^3}{3} \end{bmatrix}\begin{Bmatrix} \eta_l \\ \theta \end{Bmatrix} \tag{11}$$

A convenient dimensionless form of equation (11) is

$$\begin{Bmatrix} \overline{F} \\ \overline{M} \end{Bmatrix} = \begin{bmatrix} 12 & -6 \\ -6 & 4 \end{bmatrix}\begin{Bmatrix} \overline{\eta}_l \\ \theta \end{Bmatrix} \tag{12}$$

where

$$\overline{F} = \frac{Fl^2}{EI} \tag{13a}$$

$$\overline{M} = \frac{Ml}{EI} \tag{13b}$$

$$\overline{\eta}_l = \frac{\eta_l}{l} \tag{13c}$$

The longitudinal displacement of the free end of the beam due to bending of the beam is (ref. 3):

$$\delta_1 = \frac{1}{2}\int_0^{l} \eta'^2 d\xi \tag{14}$$

The quantity δ_1 is called the shortening of the beam due to bending.

By using $\eta(\xi)$ from equation (8),

$$\delta_1 = \frac{1}{2}\int_0^{l}\left[\left(\frac{M + Fl}{EI}\right)\xi - \frac{F}{2EI}\xi^2\right]^2 d\xi = \frac{1}{2}\left[\left(\frac{M + Fl}{EI}\right)^2\frac{l^3}{3} - \frac{F}{EI}\left(\frac{M + Fl}{EI}\right)\frac{l^4}{4} + \frac{1}{4}\left(\frac{F}{EI}\right)^2\frac{l^5}{5}\right] \tag{15}$$

Since the end load P is zero, there is no shortening due to compression. Hence, for the present case, $\delta = \delta_1$.

In dimensionless form, equation (15) becomes

$$\bar{\delta}_1 = \frac{1}{2}\left[\frac{1}{3}\left(\bar{M} + \bar{F}\right)^2 - \frac{1}{4}\bar{F}\left(\bar{M} + \bar{F}\right) + \frac{1}{20}\bar{F}^2\right] \tag{16}$$

where

$$\bar{\delta}_1 = \frac{\delta_1}{l} \tag{17}$$

Case 2; $P \neq 0$.- In this case, equation (4) takes the form

$$\frac{d^2\eta(\xi)}{d\xi^2} = \frac{1}{EI}\left\{M + F(l - \xi) - P\left[\eta_l - \eta(\xi)\right]\right\} \tag{18}$$

The solution of equation (18) with boundary conditions (6) is

$$\eta(\xi) = \frac{1}{2}\left(\frac{M + Fl - P\eta_l}{P} - \frac{F}{P}\sqrt{\frac{EI}{P}}\right)e^{\xi\sqrt{P/EI}} + \frac{1}{2}\left(\frac{M + Fl - P\eta_l}{P} + \frac{F}{P}\sqrt{\frac{EI}{P}}\right)e^{-\xi\sqrt{P/EI}}$$

$$- \frac{M + Fl - P\eta_l}{P} + \frac{F}{P}\xi \tag{19}$$

It follows that

$$\eta_l = \eta(l) = F\left(\frac{l}{P} - \frac{1}{P}\sqrt{\frac{EI}{P}}\,\frac{e^{l\sqrt{P/EI}} - e^{-l\sqrt{P/EI}}}{e^{l\sqrt{P/EI}} + e^{-l\sqrt{P/EI}}}\right) + M\left(\frac{1}{P} - \frac{1}{P}\,\frac{2}{e^{l\sqrt{P/EI}} + e^{-l\sqrt{P/EI}}}\right) \tag{20}$$

$$\theta = \eta'(l) = F\left(\frac{1}{P} - \frac{1}{P}\,\frac{2}{e^{l\sqrt{P/EI}} + e^{-l\sqrt{P/EI}}}\right) + M\left(\frac{1}{P}\sqrt{\frac{P}{EI}}\,\frac{e^{l\sqrt{P/EI}} - e^{-l\sqrt{P/EI}}}{e^{l\sqrt{P/EI}} + e^{-l\sqrt{P/EI}}}\right) \tag{21}$$

In matrix form equations (20) and (21) are

$$\begin{Bmatrix} \eta_l \\ \theta \end{Bmatrix} = \begin{bmatrix} \frac{l}{P} - \frac{1}{P}\sqrt{\frac{EI}{P}}\frac{e^{l\sqrt{P/EI}} - e^{-l\sqrt{P/EI}}}{e^{l\sqrt{P/EI}} + e^{-l\sqrt{P/EI}}} & \frac{1}{P} - \frac{1}{P}\frac{2}{e^{l\sqrt{P/EI}} + e^{-l\sqrt{P/EI}}} \\ \frac{1}{P} - \frac{1}{P}\frac{2}{e^{l\sqrt{P/EI}} + e^{-l\sqrt{P/EI}}} & \frac{1}{P}\sqrt{\frac{P}{EI}}\frac{e^{l\sqrt{P/EI}} + e^{-l\sqrt{P/EI}}}{e^{l\sqrt{P/EI}} + e^{-l\sqrt{P/EI}}} \end{bmatrix} \begin{Bmatrix} F \\ M \end{Bmatrix} \tag{22}$$

Inversion of equation (22) gives

$$\begin{Bmatrix} F \\ M \end{Bmatrix} = \frac{1}{D_1}\begin{bmatrix} \frac{1}{P}\sqrt{\frac{P}{EI}}\frac{e^{l\sqrt{P/EI}} - e^{-l\sqrt{P/EI}}}{e^{l\sqrt{P/EI}} + e^{-l\sqrt{P/EI}}} & \frac{1}{P}\frac{2}{e^{l\sqrt{P/EI}} + e^{-l\sqrt{P/EI}}} - \frac{1}{P} \\ \frac{1}{P}\frac{2}{e^{l\sqrt{P/EI}} + e^{-l\sqrt{P/EI}}} - \frac{1}{P} & \frac{l}{P} - \frac{1}{P}\sqrt{\frac{EI}{P}}\frac{e^{l\sqrt{P/EI}} - e^{-l\sqrt{P/EI}}}{e^{l\sqrt{P/EI}} + e^{-l\sqrt{P/EI}}} \end{bmatrix} \begin{Bmatrix} \eta_l \\ \theta \end{Bmatrix} \tag{23}$$

where

$$D_1 = \frac{l}{P^2}\sqrt{\frac{P}{EI}}\frac{e^{l\sqrt{P/EI}} - e^{-l\sqrt{P/EI}}}{e^{l\sqrt{P/EI}} + e^{-l\sqrt{P/EI}}} + \frac{1}{P^2}\frac{4}{e^{l\sqrt{P/EI}} + e^{-l\sqrt{P/EI}}} - \frac{2}{P^2} \tag{24}$$

The shortening due to bending is

$$\begin{aligned} \delta_1 = {} & \frac{1}{16}\left(\frac{M + Fl - P\eta_l}{P} - \frac{F}{P}\sqrt{\frac{EI}{P}}\right)^2\sqrt{\frac{P}{EI}}\left(e^{2l\sqrt{P/EI}} - 1\right) \\ & - \frac{1}{16}\left(\frac{M + Fl - P\eta_l}{P} + \frac{F}{P}\sqrt{\frac{EI}{P}}\right)^2\sqrt{\frac{P}{EI}}\left(e^{-2l\sqrt{P/EI}} - 1\right) \\ & + \frac{F}{2P}\left(\frac{M + Fl - P\eta_l}{P} - \frac{F}{P}\sqrt{\frac{EI}{P}}\right)\left(e^{l\sqrt{P/EI}} - 1\right) \\ & + \frac{F}{2P}\left(\frac{M + Fl - P\eta_l}{P} + \frac{F}{P}\sqrt{\frac{EI}{P}}\right)\left(e^{-l\sqrt{P/EI}} - 1\right) \\ & + \frac{F^2 l}{2P^2} - \frac{Pl}{4EI}\left[\left(\frac{M + Fl - P\eta_l}{P}\right)^2 - \frac{F^2 EI}{P^3}\right] \end{aligned} \tag{25}$$

In this case, however, δ_1 is not the only contribution to the shortening of the beam. The end load produces an additional shortening (or lengthening) δ_2, which is computed by the formula for compression of a bar.

$$\delta_2 = -\frac{Pl}{EA} \tag{26}$$

The total shortening (or lengthening) is then

$$\delta = \delta_1 + \delta_2 \tag{27}$$

Equations (23) and (27) determine F, M, and P if η_l, θ, and δ are known. However, P is determined only implicitly; thus, an iterative numerical solution of the equations is required. Because of the latter point, it is convenient to consider separately the two possibilities which can occur: (a) $P < 0$; (b) $P > 0$.

Case 2(a); $P < 0$.- In this case equations (23) and (27) can be put in the following dimensionless form:

$$\begin{Bmatrix} \overline{F} \\ \overline{M} \end{Bmatrix} = \frac{(kl)^2}{\overline{D}_1} \begin{bmatrix} kl\,\dfrac{\sin kl}{\cos kl} & 1 - \dfrac{1}{\cos kl} \\ 1 - \dfrac{1}{\cos kl} & \dfrac{1}{kl}\dfrac{\sin kl}{\cos kl} - 1 \end{bmatrix} \begin{Bmatrix} \overline{\eta}_l \\ \theta \end{Bmatrix} \tag{28}$$

$$\begin{aligned} \bar{\delta} = \bar{\delta}_1 + \bar{\delta}_2 = \frac{1}{2}\Bigg\{ & \frac{1}{(kl)^4}\overline{F}^2\left(1 + \frac{\sin 2kl}{2kl}\right) + \frac{1}{2(kl)^2}\left[\overline{F} + \overline{M} + (kl)^2\overline{\eta}_l\right]^2\left(1 - \frac{\sin 2kl}{2kl}\right) \\ & + \frac{\overline{F}^2}{(kl)^4} + \frac{\overline{F}}{(kl)^4}\left[\overline{M} + \overline{F} + (kl)^2\overline{\eta}_l\right]\sin^2 kl - \frac{2\overline{F}^2}{(kl)^5}\sin kl \\ & + \frac{2\overline{F}}{(kl)^4}\left[\overline{M} + \overline{F} + (kl)^2\overline{\eta}_l\right](\cos kl - 1)\Bigg\} + \frac{k^2 EI}{EA} \end{aligned} \tag{29}$$

where

$$k = \sqrt{\frac{|P|}{EA}} \tag{30}$$

$$\overline{D}_1 = k^4(EI)^2 D_1 \tag{31}$$

and D_1 is defined by equation (24).

Case 2(b); $P > 0$.- In this case equations (23) and (27) can be put in the following dimensionless form:

$$\begin{Bmatrix} \bar{F} \\ \bar{M} \end{Bmatrix} = \frac{(k\ell)^2}{\bar{D}_1} \begin{bmatrix} k\ell \dfrac{\sinh k\ell}{\cosh k\ell} & \dfrac{1}{\cosh k\ell} - 1 \\ \dfrac{1}{\cosh k\ell} - 1 & 1 - \dfrac{1}{k\ell} \dfrac{\sinh k\ell}{\cosh k\ell} \end{bmatrix} \begin{Bmatrix} \bar{\eta}_\ell \\ \theta \end{Bmatrix} \tag{32}$$

$$\bar{\delta} = \bar{\delta}_1 + \bar{\delta}_2 = \frac{1}{2}\left\{ \frac{1}{2(k\ell)^4} \bar{F}^2 \left(\frac{\sinh 2k\ell}{2k\ell} + 1 \right) + \frac{1}{2(k\ell)^2} \left[\bar{M} + \bar{F} - (k\ell)^2 \bar{\eta}_\ell \right]^2 \left(\frac{\sinh 2k\ell}{2k\ell} - 1 \right) \right.$$

$$+ \frac{1}{(k\ell)^4} \bar{F}^2 - \frac{1}{(k\ell)^4} \bar{F} \left[\bar{M} + \bar{F} - (k\ell)^2 \bar{\eta}_\ell \right] \left(\cosh^2 k\ell - 1 \right) - \frac{2}{(k\ell)^5} \bar{F}^2 \sinh k\ell$$

$$\left. + \frac{2}{(k\ell)^4} \bar{F} \left[\bar{M} + \bar{F} - (k\ell)^2 \bar{\eta}_\ell \right] (\cosh k\ell - 1) - \frac{k^2 EI}{EA} \right\} \tag{33}$$

where k is given by equation (30).

It remains to be determined whether equations (12) and (16), (28) and (29), or (32) and (33) should be used to compute $\bar{F}$, $\bar{M}$, and $k\ell$ for an arbitrary set of values of $\bar{\eta}_\ell$, θ, and $\bar{\delta}$. In other words, if $\bar{\eta}_\ell$, θ, and $\bar{\delta}$ are known, it must be determined whether $P = 0$, $P < 0$, or $P > 0$. Once this fact is known, the proper set of equations can be solved for $\bar{F}$, $\bar{M}$, and $k\ell$. To this end, consider δ_2 as given in equation (26). If $\delta_2 = 0$, then $P = 0$; if $\delta_2 > 0$, then $P < 0$; and if $\delta_2 < 0$, then $P > 0$. But by equation (27),

$$\delta_2 = \delta - \delta_1$$

Hence, $\delta = \delta_1$ implies $P = 0$; $\delta > \delta_1$ implies $P < 0$; and $\delta < \delta_1$ implies $P > 0$.

Denote the value of δ_1 for $P = 0$ by $\delta_1(0)$ and denote the value of δ_1 for $P \neq 0$ by $\delta_1(P)$. By equations (11) and (15), $\delta_1(0)$ depends only on η_ℓ and θ. For the purposes of this test only, let

$$\delta_1 = \delta_1(0) \tag{34}$$

This procedure amounts to neglecting the difference between $\delta_1(0)$ and $\delta_1(P)$. By using this assumption,

$$\delta = \delta_1(0) \rightarrow P = 0 \tag{35a}$$

$$\delta > \delta_1(0) \rightarrow P < 0 \tag{35b}$$

$$\delta < \delta_1(0) \rightarrow P > 0 \tag{35c}$$

where the arrow denotes an implication. There are heuristic arguments which indicate that the test may be rigorously valid, but no proofs have been found.

Note that the procedure does actually determine values of F, M, and P which will produce the correct values of η_l, θ, and δ.

Once F, M, and P are determined, the forces which the beam column j, j - 1 is exerting on the jth mass are given by -F, -M, and -P. The components of these forces in the inertial coordinate system are the desired quantities (fig. 1):

$$F_{X_{j,j-1}} = -P \cos \alpha_{j-1} + F \sin \alpha_{j-1} \tag{36a}$$

$$F_{Y_{j,j-1}} = -P \sin \alpha_{j-1} - F \cos \alpha_{j-1} \tag{36b}$$

$$F_{\alpha_{j,j-1}} = -M \tag{36c}$$

The same type of procedure is used to compute $F_{X_{j,j+1}}$, $F_{Y_{j,j+1}}$, and $F_{\alpha_{j,j+1}}$. In the second local coordinate system, the position and slope of the jth mass are

$$\xi_{j,j+1} = -\left(x_j - x_{j+1}\right)\cos \alpha_{j+1} - \left(y_j - y_{j+1}\right)\sin \alpha_{j+1} \tag{37a}$$

$$\eta_{j,j+1} = \left(x_j - x_{j+1}\right)\sin \alpha_{j+1} - \left(y_j - y_{j+1}\right)\cos \alpha_{j+1} \tag{37b}$$

$$\theta_{j,j+1} = \alpha_j - \alpha_{j+1} \tag{37c}$$

The total shortening is

$$\delta_{j,j+1} = l_{j,j+1} - \xi_{j,j+1} \tag{38}$$

where $l_{j,j+1}$ is the undeformed length of the beam column connecting masses j and j + 1. With the understanding that all the quantities refer to the second local coordinate system, the equations for F, M, and P are exactly as before. Hence, equations (35) are used to test δ and the proper set of equations are used to obtain F, M, and P. The forces which the beam column j, j + 1 are exerting on the jth mass are -F, -M, and -P. The components of these forces in the inertial coordinate system are (fig. 1):

$$F_{X_{j,j+1}} = P \cos \alpha_{j+1} - F \sin \alpha_{j+1} \tag{39a}$$

$$F_{Y_{j,j+1}} = P \sin \alpha_{j+1} + F \cos \alpha_{j+1} \tag{39b}$$

$$F_{\alpha_{j,j+1}} = -M \tag{39c}$$

Boundary Conditions

The boundary conditions are handled in a straightforward manner. For example, if one end of the strut is pinned, then the X- and Y-coordinates of that end are held constant while the slope of that end is allowed to vary as determined by equation (1c). In analyzing a buckling test of a single strut, the upper end of the strut is forced to descend with constant velocity while the slope of that end is determined from equation (1c). In drop tests, the foot of the strut or truss is considered to be pinned as long as it is in contact with the ground. The instant that the foot tries to leave the ground, the pin is released.

Analysis of Landing Gear Truss

A typical two-dimensional truss with shock absorbers is shown in figure 2. This truss is representative of a leg of a lunar landing vehicle for an impact in which the leg is subjected to no out-of-plane loads. The two members of the truss are joined by a pin and their upper ends are pinned to the main vehicle. The two members of the truss may be joined at the foot, or in the section of the main strut below the shock absorber, or, as shown in figure 2, in the section of the main strut above the shock absorber.

The analytical model of the truss can have up to 25 masses, including one mass for the center of mass of the vehicle. A shock absorber can be located between any two adjacent masses of the main strut and a second shock absorber can be located between any two consecutive masses of the secondary strut. The following definitions are needed in connection with the analytical model:

c_1 subscript indicating point on main strut to which secondary strut is joined

k_1 subscript indicating point at vehicle end of main strut

k_1+1 subscript indicating point at vehicle end of secondary strut

c_2 subscript indicating point at end of secondary strut which attaches to main strut

A typical analytical model of the truss using 11 mass points is shown in figure 3.

The procedures discussed previously for a strut have been incorporated into a procedure for dynamic analysis of the two-dimensional truss. The method is first extended to a truss without shock absorbers; generalization to include shock absorbers is done subsequently.

Consider, first, the pinned joint connecting the two struts. The equations of motion for the joint are as follows:

$$\left(m_{c_1} + m_{c_2}\right)\ddot{x}_{c_1} = F_{X_{c_1,c_1-1}} + F_{X_{c_1,c_1+1}} + F_{e,X_{c_1}} \tag{40a}$$

$$\left(m_{c_1} + m_{c_2}\right)\ddot{y}_{c_1} = F_{Y_{c_1,j-1}} + F_{Y_{c_1,c_1-1}} + F_{e,Y_{c_1}} \tag{40b}$$

$$I_{c_1}\ddot{\alpha}_{c_1} = F_{\alpha_{c_1,c_1-1}} + F_{\alpha_{c_1,c_1+1}} \tag{40c}$$

$$\ddot{x}_{c_2} = \ddot{x}_{c_1} \tag{40d}$$

$$\ddot{y}_{c_2} = \ddot{y}_{c_1} \tag{40e}$$

$$I_{c_2}\ddot{\alpha}_{c_2} = F_{\alpha_{c_2,c_2-1}} \tag{40f}$$

Equations (40a) and (40b) imply that the position, velocity, and acceleration of the joint are determined by adding the forces from the three beam columns connected to the joint and integrating the resulting equations. Equations (40d) and (40e) express the fact that point c_2 on the secondary strut coincides with point c_1 on the main strut insofar as the x and y motion is concerned. Equations (40c) and (40f) indicate the fact that the moments on the main and secondary struts do not couple because of the pin.

The motion of the center of mass of the vehicle is determined by the forces and torques exerted by the two pinned joints connecting the struts to the main vehicle. The two upper ends of the struts and the vehicle center of mass are considered to be rigidly connected. The motion of the center of mass of the vehicle is governed by the following equations (fig. 4):

$$m_{cm}\ddot{x}_{cm} = F_{t,X_{k_1}} + F_{t,X_{k_1+1}} + F_{e,X_{cm}} \tag{41a}$$

$$m_{cm}\ddot{y}_{cm} = F_{t,Y_{k_1}} + F_{t,Y_{k_1+1}} + F_{e,Y_{cm}} \tag{41b}$$

$$I_{cm}\ddot{\alpha}_{cm} = F_{t,X_{k_1}}\left(y_{cm} - y_{k_1}\right) + F_{t,Y_{k_1}}\left(x_{k_1} - x_{cm}\right) + F_{t,X_{k_1+1}}\left(y_{cm} - y_{k_1+1}\right) + F_{t,Y_{k_1+1}}\left(x_{k_1+1} - x_{cm}\right) \tag{41c}$$

where excluding the impacting leg

m_{cm} mass of vehicle

x_{cm}, y_{cm} coordinates of center of mass of vehicle

I_{cm} moment of inertia of vehicle

$F_{e,X_{cm}}, F_{e,Y_{cm}}$ components of external force at vehicle center of mass

F_{t,X_j}, F_{t,Y_j} components of total force (elastic plus external) at mass j

Note that equations (41) are coupled with equations (1).

The coordinates of masses k_1 and $k_1 + 1$ are determined from the vehicle center of mass coordinates by the following equations for the vehicle orientation shown in figure 4:

$$x_{k_1} = x_{cm} + d_1 \cos \alpha_{cm} \tag{42a}$$

$$y_{k_1} = y_{cm} + d_1 \sin \alpha_{cm} \tag{42b}$$

$$x_{k_1+1} = x_{cm} + d_2 \cos(\alpha_{cm} + \theta_{cm}) \tag{42c}$$

$$y_{k_1+1} = y_{cm} + d_2 \sin(\alpha_{cm} + \theta_{cm}) \tag{42d}$$

where

d_1 distance between vehicle center of mass and mass k_1

d_2 distance between vehicle center of mass and mass $k_1 + 1$

θ_{cm} angle subtended at vehicle center of mass by masses k_1 and $k_1 + 1$

Procedure for Incorporating Shock Absorbers

For many applications, it is desirable to include a load-limiting shock absorber in a strut. A typical shock absorber of this type contains cartridges of crushable aluminum honeycomb. These shock absorbers are assumed to produce a constant force while stroking in either direction. The inclusion of such a shock absorber in the present analysis is accomplished as follows. The shock-absorber force is computed as a reaction force to the end load P. If the compressive load in the section of strut containing the shock absorber is less than the crush load of the cartridges, the shock-absorber force is set equal to the compressive load, and stroking is not considered to have occurred. If the compressive load is computed to be greater than or equal to the crush load, the shock-absorber force is set equal to the crush load, stroking occurs, and the reference length of the shock-absorber section is readjusted to a new shortened length. Once the shock absorber has shortened and then started to open, a small frictional force is applied until the shock absorber opens out to its original length. Then, if the shock absorber

continues to open, the extensional shock-absorber force is applied in a manner analogous to the compressive shock-absorber force.

Note that there are two end loads associated with each section of the strut. For example, in figure 3, consider the section of strut connecting masses 2 and 3. There will be an end load $P_{2,3}$ acting at mass 2 as seen in the local coordinate system attached to mass 3; and there will be an end load $P_{3,2}$ acting at mass 3 as seen in the local coordinate system attached to mass 2. Stroking is considered to occur only if both of these forces are greater than or equal to the crush load.

In any attempt to analyze the response of a specific system, some modification and generalization of these shock absorbers will undoubtedly be necessary. The present shock absorber was considered in order to demonstrate the capability of this type of analysis to include shock absorbers of the load-limiting type.

NUMERICAL SOLUTIONS

Solution of Force Equations

As stated earlier, for $P \neq 0$, equations (23) and (27) must be solved numerically for F, M, and P. The solution can be obtained on a digital computer by using standard numerical techniques. However, these techniques, which require several iterations to achieve the desired accuracy, result in large amounts of computer time. Therefore, the following procedure has been used to determine the solution. This scheme determines values of F, M, and P which are well within the required accuracy and can reduce computer time by a factor of 10 or more. From equations (26) and (27),

$$\delta = \delta_1 - \frac{P\ell}{EA}$$

Hence,

$$\left|P\ell\right| = EA\left|\delta - \delta_1\right|$$

By equation (30),

$$k^2(EI)\ell = EA\left|\delta - \delta_1\right|$$

$$(k\ell)^2 = \frac{\ell(EA)}{EI}\left|\delta - \delta_1\right|$$

$$k\ell = \sqrt{\frac{\ell^2(EA)}{EI}\left|\bar{\delta} - \bar{\delta}_1\right|} \tag{43}$$

Now $\bar{\delta}_1$, which is the shortening of the beam due to bending, changes very little from one time increment to the next. Therefore, as a first approximation to $k\ell$,

$$k\ell \approx \sqrt{\frac{\ell^2(EA)}{EI}\left|\bar{\delta} - \bar{\delta}_1(x)\right|} \tag{44}$$

where $\bar{\delta}_1(x)$ is the value of $\bar{\delta}_1$ from the previous time increment. For case 2(a), $\bar{\delta}_1(x)$ is determined from equation (29); for case 2(b), $\bar{\delta}_1(x)$ is determined by equation (33). The value of $k\ell$ as determined in this manner could be used in the right-hand side of equation (43) to compute a second approximation, and so on until the desired accuracy is achieved. However, because $\bar{\delta}_1$ changes only slightly from one time increment to the next, results have shown that the first value of $k\ell$ is sufficiently accurate and no further iterations are necessary. Once $k\ell$ is determined, $\overline{F}$ and $\overline{M}$ are computed by equations (28) for case 2(a) ($P < 0$) or by equations (32) for case 2(b) ($P > 0$). Then F, M, and P are determined from equations (13a), (13b), and (30), where the sign of P must be chosen consistent with the appropriate case. The values of F, M, and P as thus determined do, in fact, produce the proper values of η_ℓ, θ, and δ to a satisfactory degree of approximation.

Integration Scheme

The numerical integration of equations (1) is carried out by using Euler's method. This very simple scheme has been used effectively on other problems of this same type (ref. 1). It has the advantages of being self-starting and of requiring only one evaluation of the derivatives. Since the evaluation of the derivatives requires a considerable amount of computing time, this latter point is believed to outweigh any advantages of more sophisticated schemes, such as Runge-Kutta, which require several evaluations of the derivatives on each step. The inclusion of higher order differences in the present scheme (Adams method) produces a slight increase in accuracy. The equations for Euler's method are

$$x(t + \Delta t) = x(t) + \Delta t\, \dot{x}(t)$$

$$\dot{x}(t + \Delta t) = \dot{x}(t) + \Delta t\, \ddot{x}(t)$$

Equation (1c) requires special treatment for accurate numerical integration. The parameter I_j which appears in equation (1c) is the rotary inertia of the jth mass. Rotary inertia was included not because it was important, but because equations (1) were the simplest way to arrive at a consistent set of equations of motion. Equation (1c) could be completely eliminated from the analysis. However, the elimination of this equation would require an iterative method to determine the α_j values.

When compared with motion in the x- and y-directions, the α-motion has very little inertial lag. The α-acceleration is much larger than the accelerations in the x- and y-directions. Also, the α-coordinate of a mass point oscillates at a much higher frequency than the x,y-coordinates. These high-frequency oscillations require an extremely

small time increment for accurate numerical integration and result in unduly long computer runs. To reduce the computer time, an impulsive damper was introduced into the α-motion. The action of the impulsive damper is explained in the following section.

Impulsive Damper

The behavior of $\ddot{\alpha}$ both with and without the impulsive damper is shown in figure 5 for small values of the rotary inertia I_j. Without the impulsive damper, $\ddot{\alpha}$ diverges very rapidly because of numerical instability of the integration scheme. If a time increment about one fiftieth as big were used, $\ddot{\alpha}$ would oscillate nearly harmonically with a maximum amplitude about equal to the first negative peak of the broken line.

The solid line shows the influence of the impulsive damper. As the solution begins, α is most generally not in its instantaneous equilibrium position and an acceleration moves α toward its instantaneous equilibrium position. At this stage of the problem, the two curves are identical. Since α is moving toward its instantaneous equilibrium position, the computation is allowed to proceed normally. In the process of moving to its instantaneous equilibrium position, α acquires a finite velocity increment. Therefore, once α reaches its instantaneous equilibrium position, this velocity will cause α to overshoot and begin to oscillate. In order to damp out the oscillation, the α velocity is set equal to zero once α reaches its instantaneous equilibrium position. This procedure amounts to adding a ficticious impulsive moment to the system which is just enough to reduce the α velocity to zero. Thus, α is prevented from overshooting and is actually stopped in its instantaneous equilibrium position. As the solution progresses, the instantaneous equilibrium value of α changes. When this happens, α is accelerated again and the entire process is repeated. As shown in figure 5, α can have very high accelerations even with the impulsive damper. The high accelerations indicate that the instantaneous equilibrium value of α is changing rapidly and α is lagging behind. Once α reaches its new instantaneous equilibrium position, the high accelerations are damped out. It is essential, of course, that α remains as near as possible to its instantaneous equilibrium position since, for small values of I_j, α reaches its new position almost instantaneously. For this reason, periodic checks must be made to assure that α is not lagging too far behind. In the cases so far considered, α has been found to follow along satisfactorily for sufficiently small values of I_j. As I_j increases in magnitude, the damping effect becomes more pronounced. An example is shown in figure 6. The upper plot is a time history of the deflection of the center of a vertical strut with shock absorber which is oscillating in the lateral direction. The lower plot is a time history of the α-coordinate of the lower end of the strut.

One additional point should be mentioned. The time increment used in the numerical integration must be many times smaller than the period of the highest natural frequency of the x- and y-motion. This statement remains true even if more sophisticated

numerical integration procedures are employed. Hence, if the period of the highest natural frequency of the truss under consideration is short compared with the time period of interest then a large amount of computer time may be necessary. This condition can occur even when the period of interest is as short as 0.1 second. For a system with ten masses representing the truss and one mass for the vehicle, the computer program requires approximately 0.075 second per iteration on an IBM 7094 computer. This fact appears to be the most restrictive limitation of the method.

APPLICATIONS

Buckling of Beam Column

To check the validity of the method presented in this paper, a comparison was made to results obtained by Hoff in reference 4. The accuracy of Hoff's results has been discussed by Sevin in reference 5. The system which was analyzed is a beam column pinned at both ends as shown in figure 7. The piston at the upper end of the beam column is forced to descend at a constant velocity of 0.256 inch per second (0.00650 m/sec). The case analyzed represents a very rapid loading of a slender beam column. In the work of Hoff and Sevin, the beam column had a small initial curvature. Since the present analysis does not account for initial deviations from straightness, the beam column was considered to be initially straight and it was given a small lateral velocity at the center. For this reason, the comparison of results shown in figure 8 indicate the same general type of behavior but not the same numerical magnitudes. A three-mass approximation of the beam column was used. The comparisons are presented in terms of the nondimensional parameters used by Hoff.

The dashed curves in figure 8 show the results of the present analysis for an initial lateral velocity of 0.5 inch per second (0.0127 m/sec). Although different values of the initial lateral velocity produce different curves, the results shown are typical. In the initial phase of the problem, the inertia of the beam column causes the lateral deflection of the center of the column to lag behind the static values. Eventually, this inertial lag is overcome and the final part of the solution consists of an oscillation about the static curve. Note that the axial load in the beam column reaches the Euler buckling load at a dimensionless time of 1.0. Hence, failure of an actual beam column should occur very close to this time.

It should be pointed out that equations (28) are singular if the end load P is equal to the Euler buckling load. However, this difficulty occurs only if P is exactly at the critical value, or at least extremely close to it. In actual practice, the value of P was never close enough to the exact critical value to cause any difficulties. The equations were simply integrated right through the singularity. In actual physical problems the

singularity should not cause any difficulties because the axial load in a beam column will ordinarily be kept well below the buckling load.

The next example illustrates the onset of dynamic buckling. A beam column is said to buckle dynamically if the amplitude of the vibrations tend to grow without limit (ref. 4). Behavior of this type is shown in figure 9 for three different cases. The number of lateral oscillations which the column undergoes before buckling is dependent upon the velocity of the descending piston. The midpoint lateral deflections of the center of the beam column for three different values of the velocity of the descending piston are shown in figure 9. Prior to the onset of dynamic buckling, the number of oscillations which are predicted from the formula given by Hoff are approximately as follows: 1/3 oscillation for a velocity of the descending piston of 0.256 inch per second (0.00650 m/sec); 2/3 oscillation for a velocity of the descending piston of 0.128 inch per second (0.00325 m/sec); $1\frac{1}{3}$ oscillations for a velocity of the descending piston of 0.064 inch per second (0.001625 m/sec). In figure 9, the horizontal dashed lines indicate the region of normal vibrations. As the data in figure 9 indicate, the present analysis is in agreement with the values predicted by Hoff. For a velocity of the descending piston of 0.256 in./sec (0.00650 m/sec) buckling occurs before the midpoint of the beam column begins to swing back toward its initial position; for a velocity of the descending piston of 0.128 in./sec (0.00325 m/sec), the midpoint of the beam column begins to swing back and then buckles out; for a velocity of the descending piston of 0.064 in./sec (0.001625 m/sec), the midpoint swings out, comes back, and finally buckles out on the opposite side.

Buckling of Impacting Strut

Figure 10 shows a strut with a shock absorber and its analytical model. The strut is of the general type presently being considered for the landing gear of the lunar module. The strut is made of aluminum, is 12.3 ft (3.749 m) long and 6 inches (0.1524 m) in diameter, and has a wall thickness of about 0.03 inch (0.000762 m). At the upper end of the strut there is a heavy mass which weighs approximately 16 percent of the Euler buckling load. The shock absorber is a capsule of aluminum honeycomb with a crush load of 3800 pounds (16903.24 N). Figure 11 shows a typical load-deflection curve which results from the analytical model of the shock absorber as described in a previous section. Note that the assumption of small deflections is valid because the length of the shock-absorber section is readjusted to a new shortened length as the shock absorber crushes.

Figure 12 shows the lateral displacements of the center of the strut without shock absorbers for various values of the impact velocity. The strut is dropped straight down and the bottom of the strut is stopped instantaneously when it touches the ground. The center masses of the strut are given a small lateral velocity in order to induce bending. At $t = 0$, the bottom of the strut first contacts the ground.

For an impact velocity of 1 ft/sec (0.3048 m/sec) the maximum axial load in the strut is well below the buckling load and there is no pronounced effect on the lateral vibrations. With an impact velocity of 2 ft/sec (0.6096 m/sec) the maximum axial load slightly exceeds the Euler buckling load. Before buckling begins, however, the downward velocity of the heavy mass at the upper end of the strut is stopped at approximately 0.02 second. As the strut begins to rebound, the upward displacement of the heavy mass at the upper end of the strut begins to relieve the compressive load. For impact velocities greater than 2 ft/sec (0.6096 m/sec), the effect on the lateral displacements is clearly evident in figure 12.

Figure 13 shows the lateral vibrations of the strut with shock absorbers impacting at 2 ft/sec (0.6096 m/sec). The center of the strut reaches its maximum lateral displacement on the first vibration and then oscillates with decreasing amplitude. The downward motion of the large mass is not stopped until about 0.076 second. Buckling is prevented by the shock absorber, which limits the axial load on the strut. The shock absorber begins stroking at approximately 0.004 second and stops stroking at approximately 0.076 second. The lateral deflection of the strut without shock absorbers impacting at 1 ft/sec (0.3048 m/sec) is shown by the dashed line in figure 13 for comparison. For the strut without shock absorbers impacting at 1 ft/sec (0.3048 m/sec), the downward motion of the heavy mass is stopped at approximately 0.021 second.

Effect of Lateral Elasticity on Impacting Strut

As shown by the tests and supporting analysis of a 1/6-scale model of a lunar-module-type spacecraft described in reference 2, stored elastic energy can significantly affect the landing dynamics of lunar-landing vehicles. However, the analysis reported in reference 2 did not include lateral elasticity.

To determine the effect of lateral elasticity, the strut described in the previous section was impacted at 2 ft/sec (0.6096 m/sec) with varying amounts of axial and lateral elasticity. The initial lateral velocities of the center of the strut were varied from case to case in order to produce different amounts of maximum lateral displacement of the center of the strut. A maximum lateral deflection of 1 inch (2.54 cm) corresponds to an axial stress which exceeds the manufacturer's recommendation for the ultimate stress.

For the strut considered, the results indicate that axial elasticity is much more important than lateral elasticity in the dynamic behavior of the impacting strut. In figure 14, the maximum upward momentum of the rebounding heavy mass at the upper end of the strut is plotted against the maximum lateral amplitude of the center of the strut for different values of axial and lateral stiffness. As figure 14 shows, reducing EI by a factor of 2 or 3 has very little effect on the maximum upward momentum. However, reducing EA by a factor of 2 increases the maximum upward momentum by almost

40 percent. The figure also indicates that lateral vibrations have only a very slight effect on the maximum upward momentum.

In figure 15, vertical-acceleration time histories are shown for four of the extreme conditions presented in figure 14. Here also it can be seen that the reduction in EI produces only a small change in the vertical-acceleration time history whereas the reduction in EA produces a much larger change in the curve.

Impact of Vehicle With Truss-Type Landing Gear

Figure 16 shows a two-dimensional vehicle with a truss-type leg. The truss consists of two nearly equal struts joined at the foot. The struts are essentially the same as the strut considered above. The vehicle mass is approximately that of the lunar module at the moment of impact on the lunar surface. Lunar gravity is used. The vehicle impacts on one leg only. Calculation is stopped prior to impact of another leg. An impact velocity of 1 ft/sec (0.3048 m/sec) is used. This velocity is just enough to build up the loads in the struts to the crush loads of the shock absorbers (3800 lb or 16 903.24 N).

In figure 17, the vertical-acceleration time history of the center of mass of the vehicle is shown for three different cases. For the first case, the full values of EI and EA are used for both struts. The second case shows the effect of reducing the EI of both struts by a factor of two while keeping EA at its full value. As the figure shows, these two curves are practically identical. The third case shows the vertical-acceleration time history of the vehicle center of mass when the EA of both struts is reduced by a factor of two and EI is maintained at its full value. In this case, the curve is considerably changed and exhibits the same characteristics as for a single strut dropped straight down. The horizontal-acceleration response time histories show effects very similar to the vertical acceleration.

These results show that for the vehicle considered, a change in the bending stiffness by a factor of two produces essentially no change in the acceleration time history of the center of mass, and thus indicates that the motion of the vehicle is not substantially affected by the lateral vibrations of the landing gear. However, a change of the same amount in the longitudinal stiffness results in a much different acceleration time history of the vehicle center of mass. This result indicates that for the case analyzed, the longitudinal elasticity of the landing gear is much more important in the impact dynamics of the vehicle than the lateral elasticity.

CONCLUDING REMARKS

A method has been developed for analyzing the dynamic behavior of two-dimensional impacting struts and trusses which may contain load-limiting shock

absorbers. Lumped masses and finite elastic elements are used to represent the system and response time histories are obtained for each mass point. Application of the method to an impacting strut of the general type presently being considered for the landing gear of the lunar module indicates that the impact dynamics is essentially unaffected by variations in lateral elasticity. However, the impact dynamics is affected by variations in axial elasticity. Thus, axial elasticity is much more important than lateral elasticity in the dynamic behavior of the impacting strut. A similar conclusion is obtained for a vehicle with a specific truss-type landing gear constructed of these struts.

The present limitation of the method is the large amount of computer time required for systems which have a high natural frequency with a period which is very short compared with the time period of interest.

Langley Research Center,
National Aeronautics and Space Administration,
Langley Station, Hampton, Va., November 28, 1967,
124-08-04-13-23.

REFERENCES

1. Walton, William C., Jr.; and Durling, Barbara J.: A Procedure for Computing the Motion of a Lunar Landing Vehicle During the Landing Impact. NASA TN D-4216, 1967.

2. Herr, Robert W.; and Leonard, H. Wayne: Dynamic Model Investigation of Touchdown Stability of Lunar-Landing Vehicles. NASA TN D-4215, 1967.

3. Timoshenko, Stephen P.; and Gere, James M.: Theory of Elastic Stability. Second ed., McGraw-Hill Book Co., Inc., c.1961.

4. Hoff, N. J.: The Dynamics of the Buckling of Elastic Columns. J. Appl. Mech., vol. 18, no. 1, Mar. 1951, pp. 68-74.

5. Sevin, Eugene: On the Elastic Bending of Columns Due to Dynamic Axial Forces Including Effects of Axial Inertia. Trans. ASME, Ser. E, J. Appl. Mech., vol. 27, no. 1, Mar. 1960, pp. 125-131.

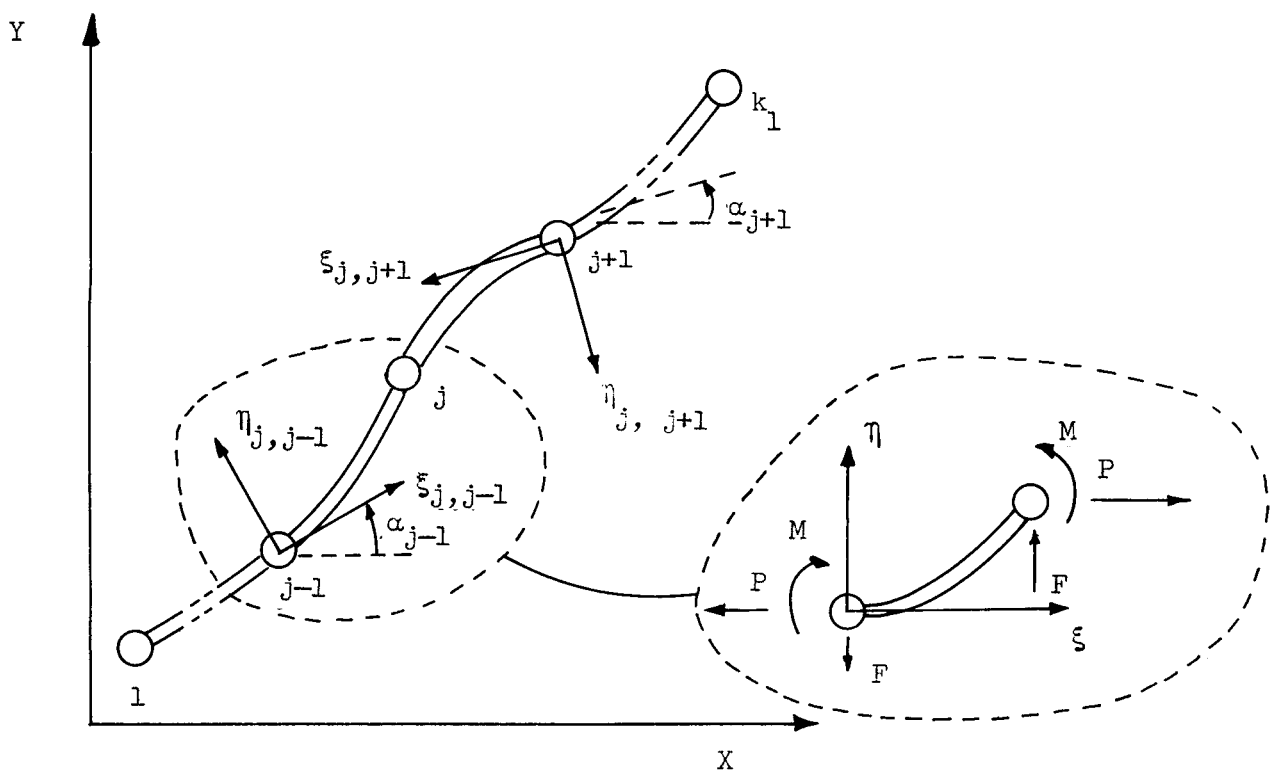

Figure 1.- Coordinate systems. Dashed lines encircle isolated section.

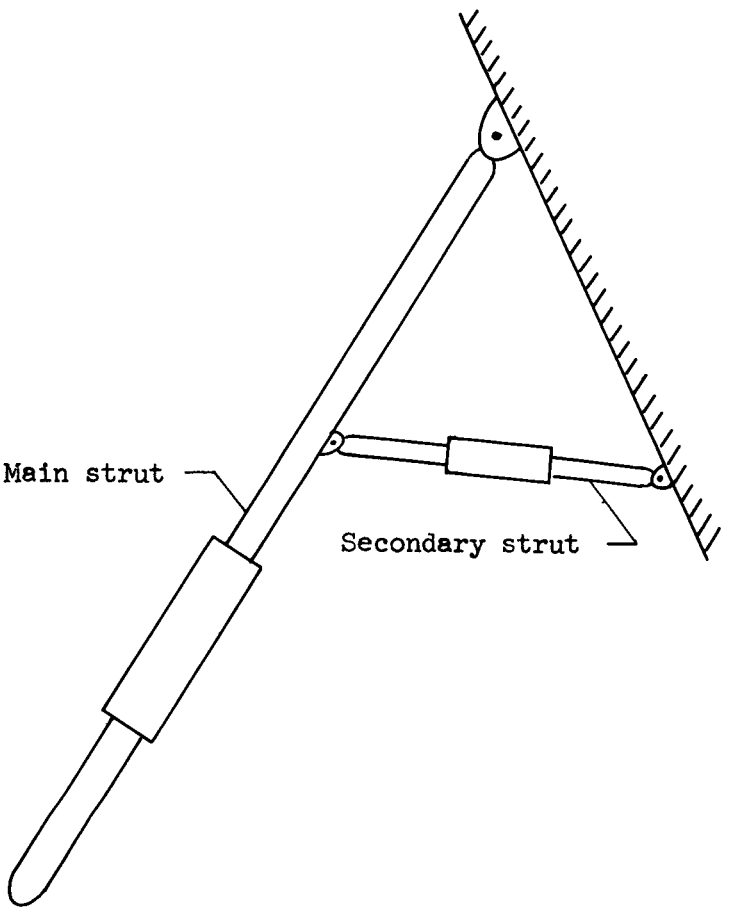

Figure 2.- Typical two-dimensional truss with shock absorbers.

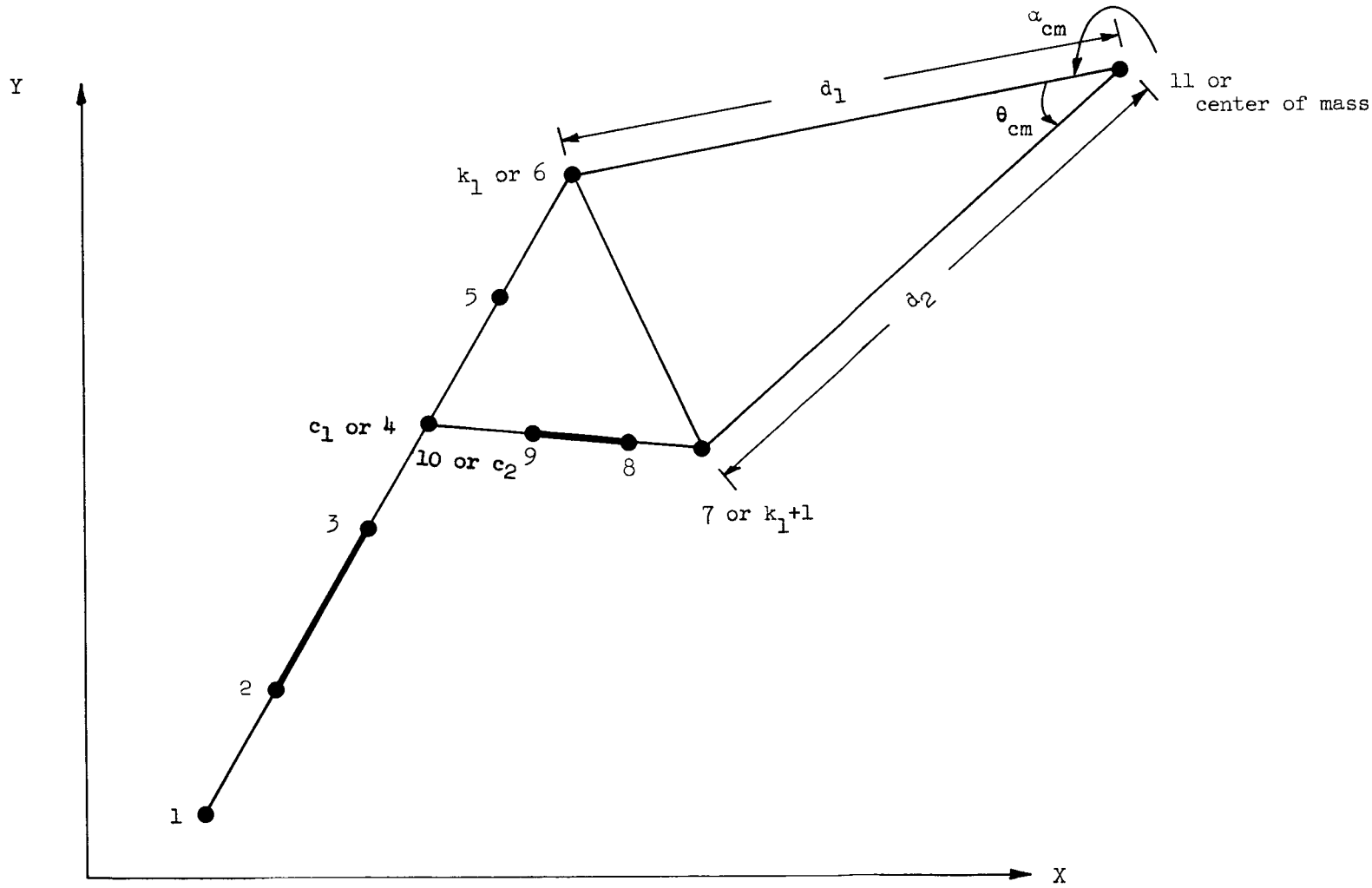

Figure 3.- Typical analytical model of truss.

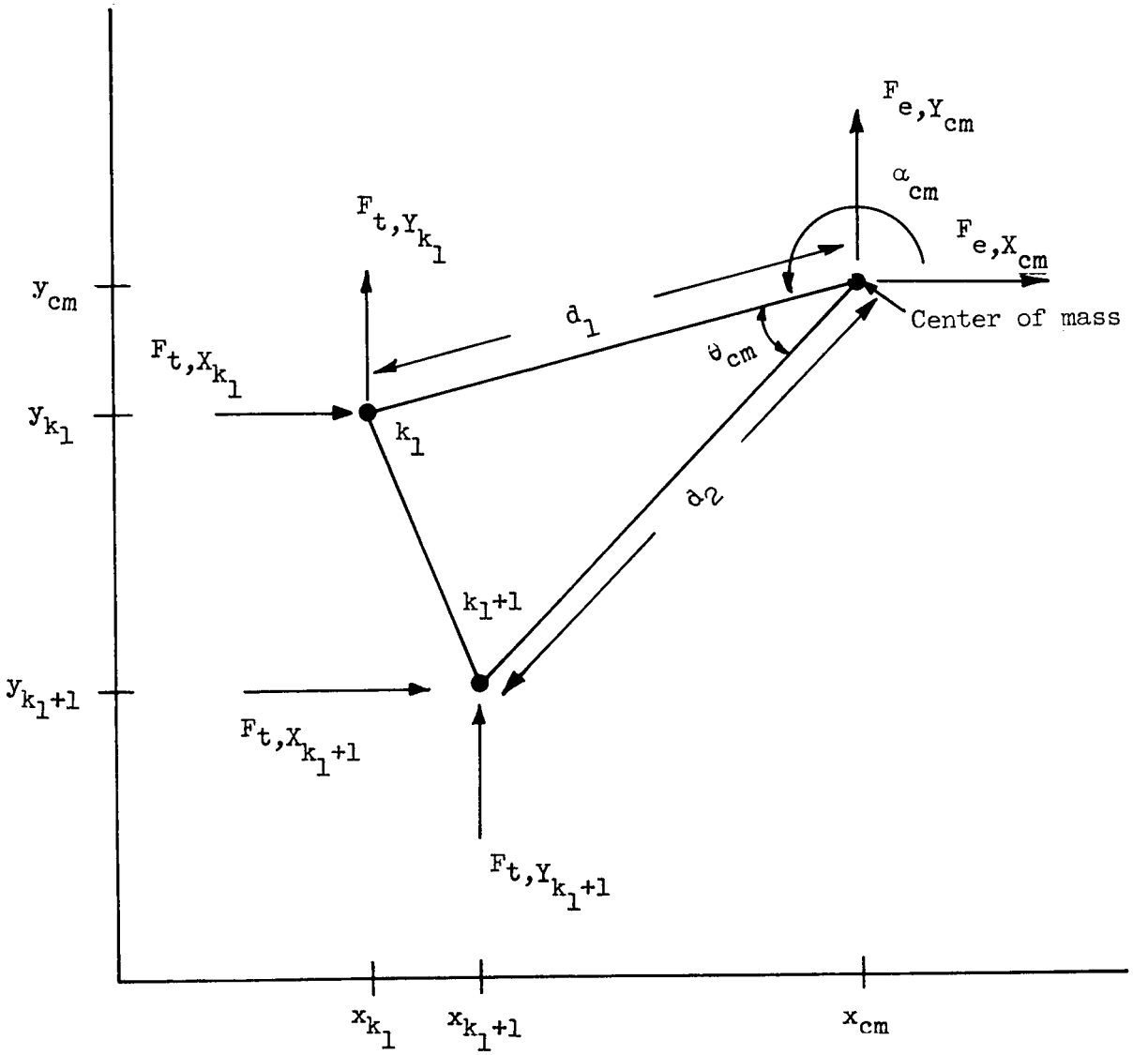

Figure 4.- Forces acting on vehicle center of mass.

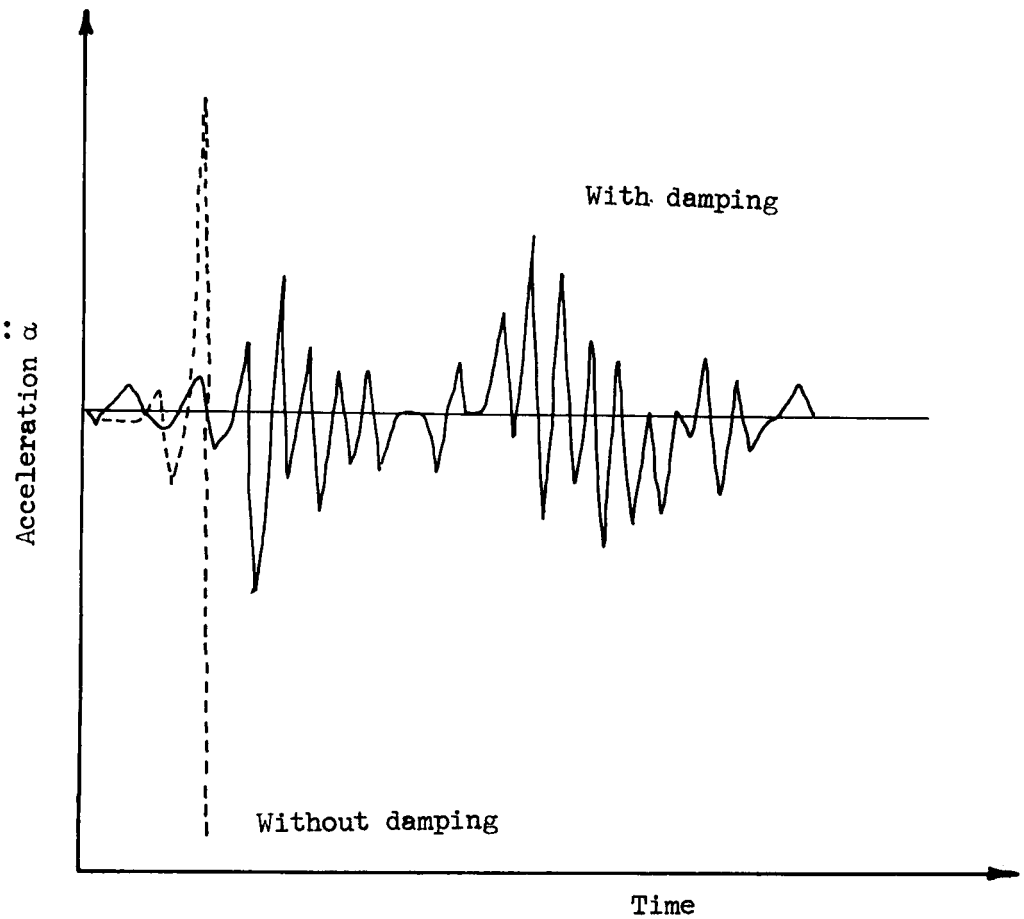

Figure 5.- Effect of fictitious impulsive damper for a typical problem.

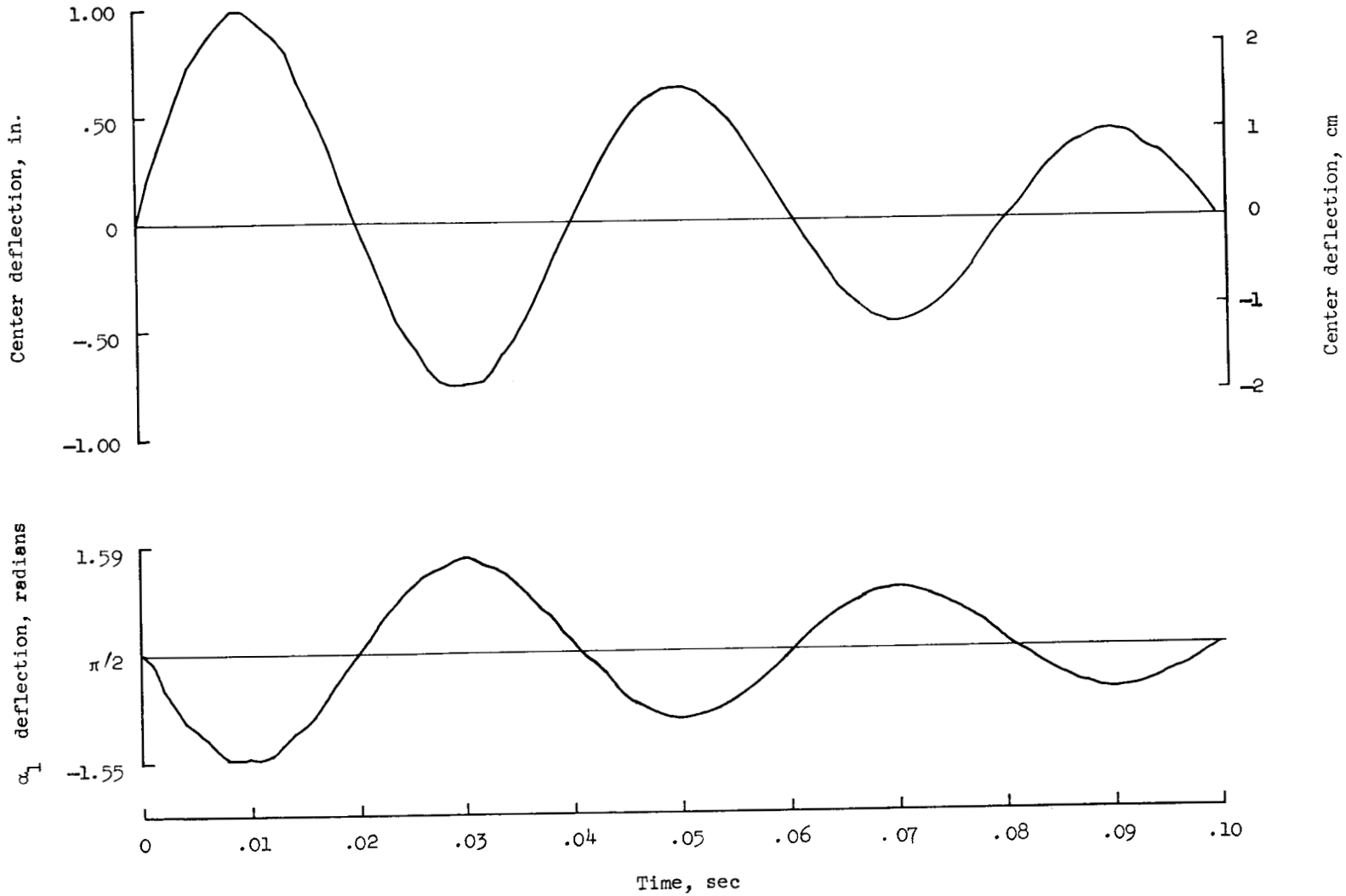

Figure 6.- Time history of slope of lower end of vertical strut and time history of lateral deflection of center.

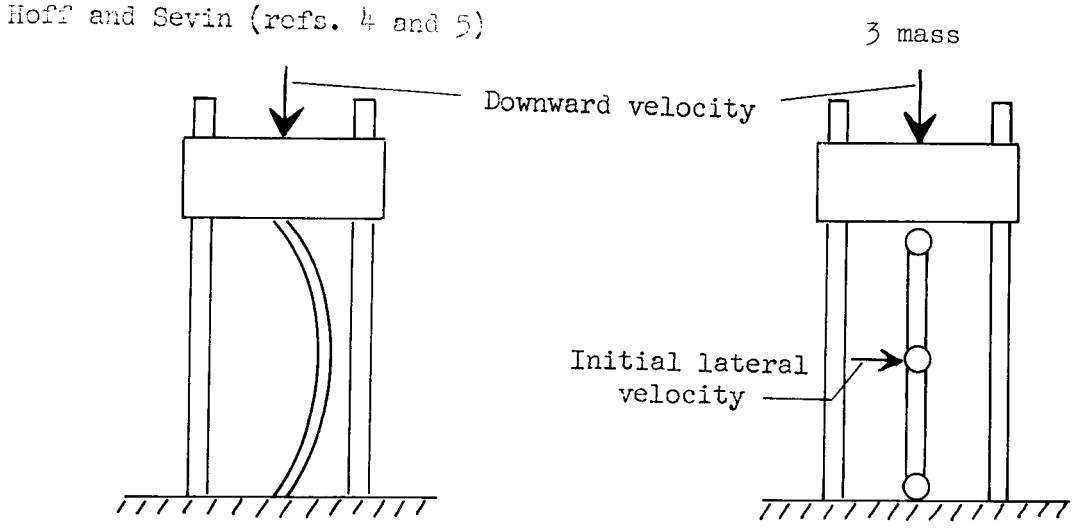

Figure 7.- Buckling test used for comparison of results.

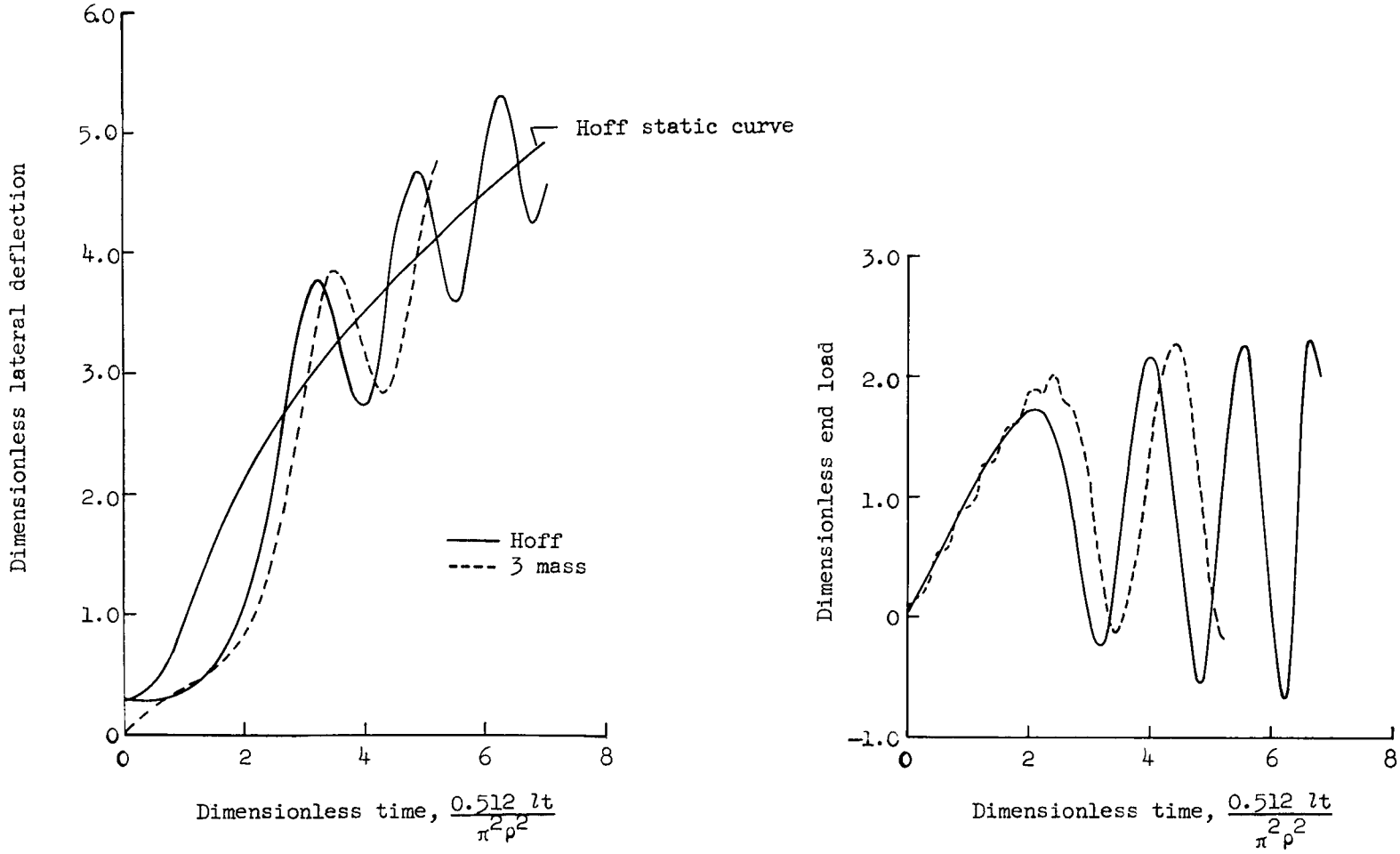

Figure 8.- Comparison of three-mass buckling test with results obtained by Hoff.

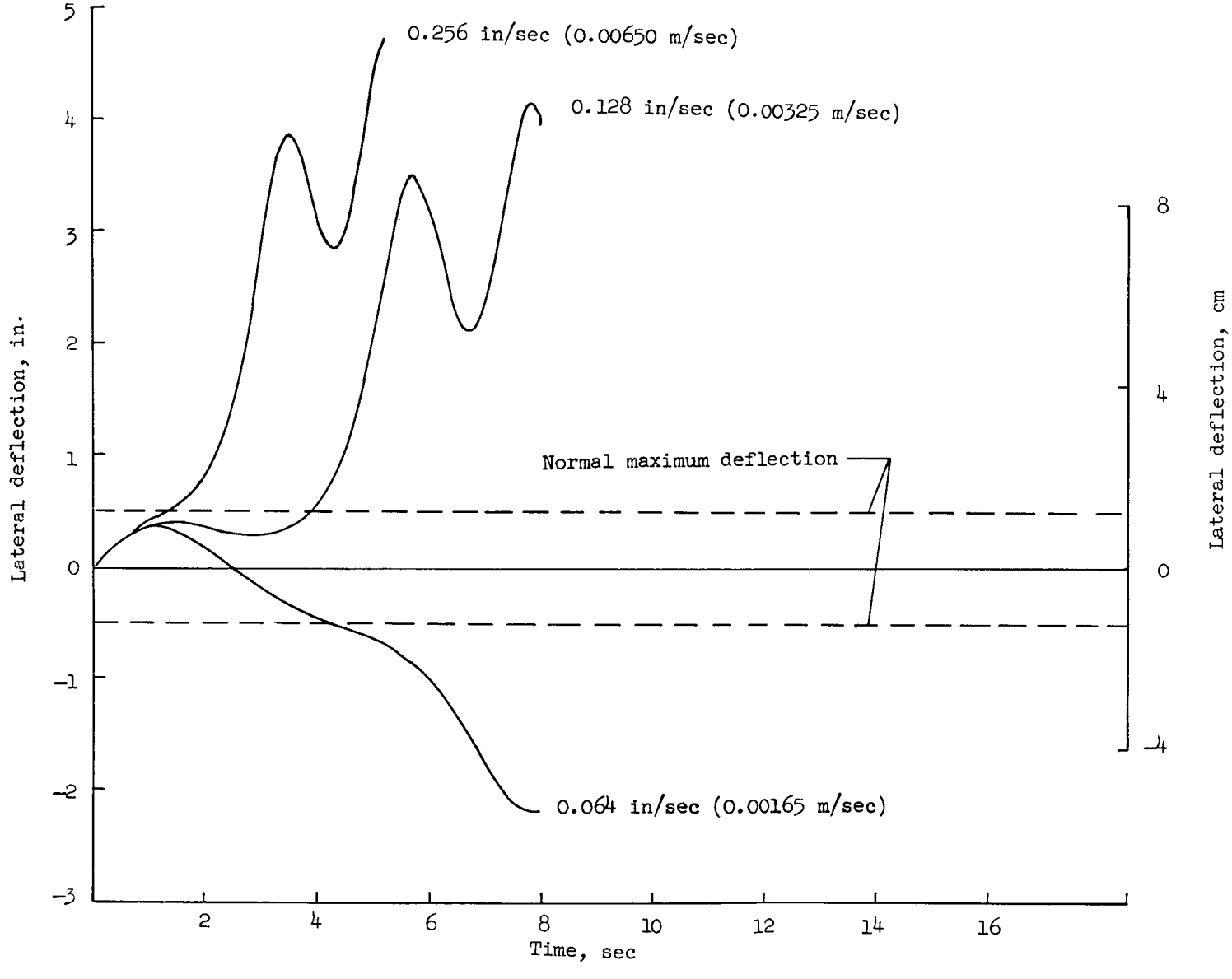

Figure 9.- Effect of velocity of descending piston on lateral deflection.

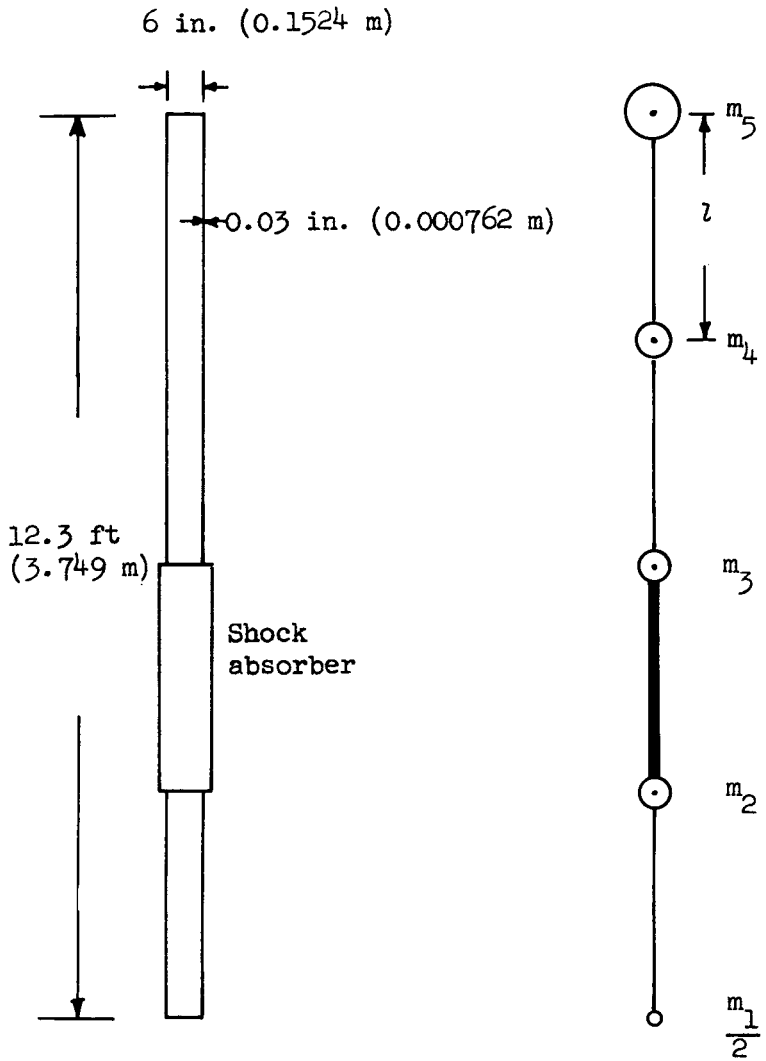

m_5 = 5.2117 slugs = 76.059 kg

m_1 to m_4 = 0.0068 slugs = 0.0992 kg

EI = 29.2898×10^6 lb–in.^{2} = 840.5587 N–m^2

EA = 6.122×10^6 lb = 27.232×10^6 N

l = 36.885 in. = 0.9368 m

Figure 10.- Strut with shock absorber and its analytical model.

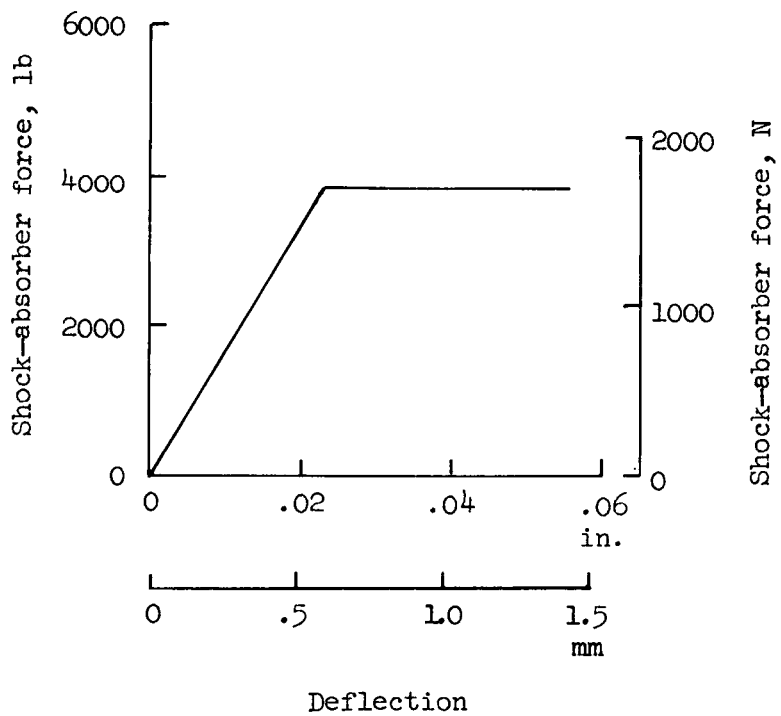

Figure 11.- Typical compressive load-deflection curve for analytical model of shock-absorber cartridge.

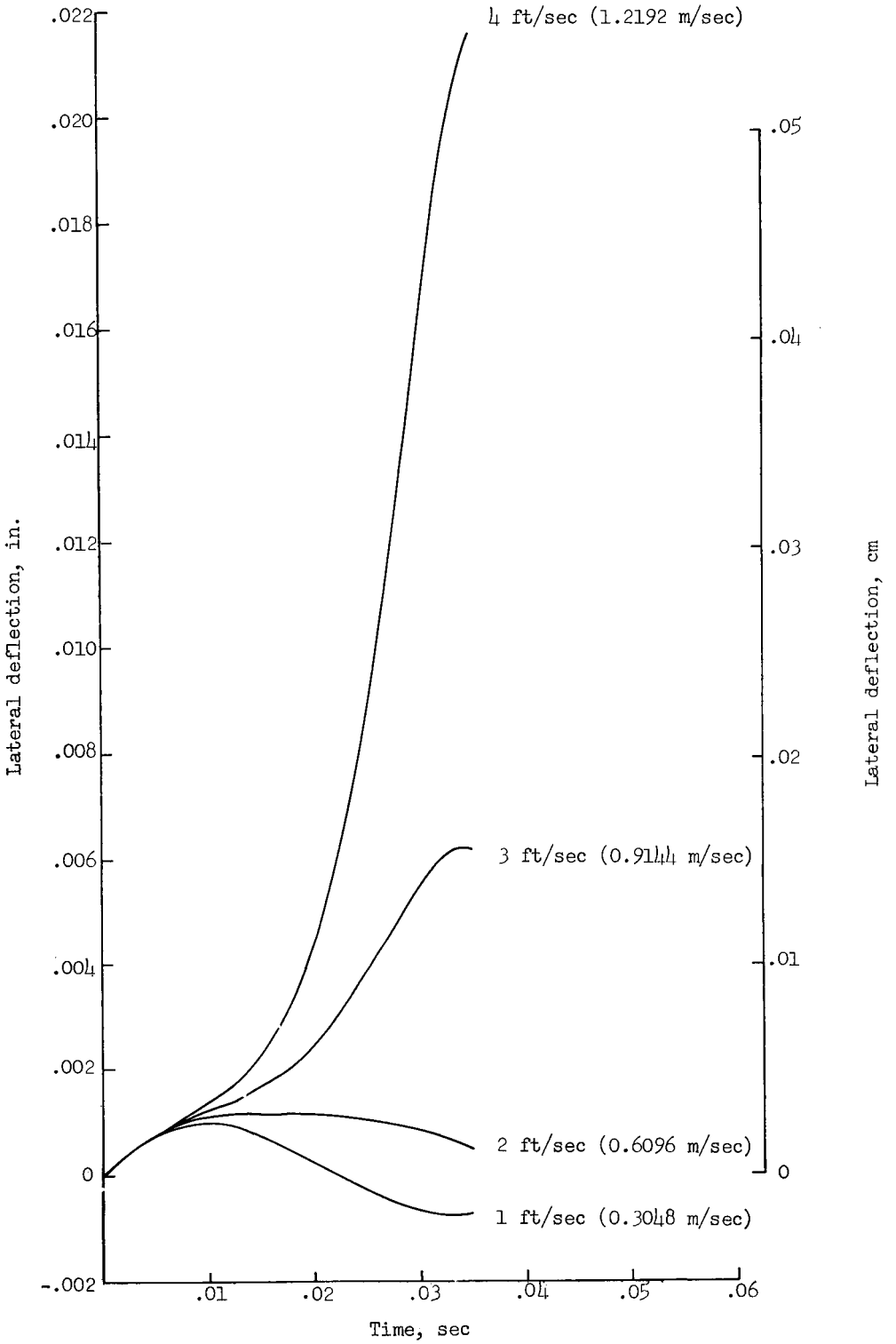

Figure 12.- Lateral deflection of center of impacting strut without shock absorbers for various impact velocities.

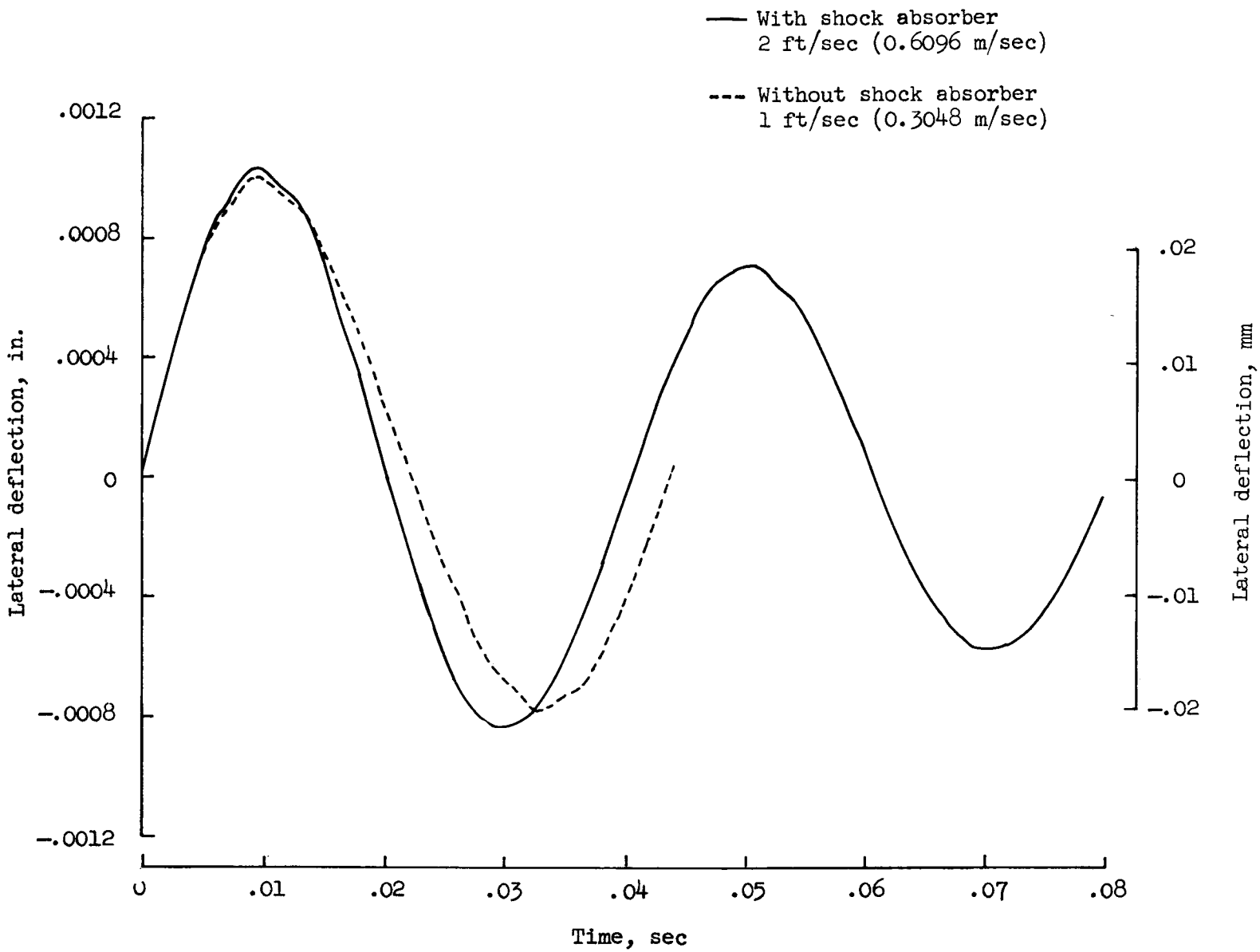

Figure 13.- Lateral deflection of center of impacting strut with and without shock absorbers.

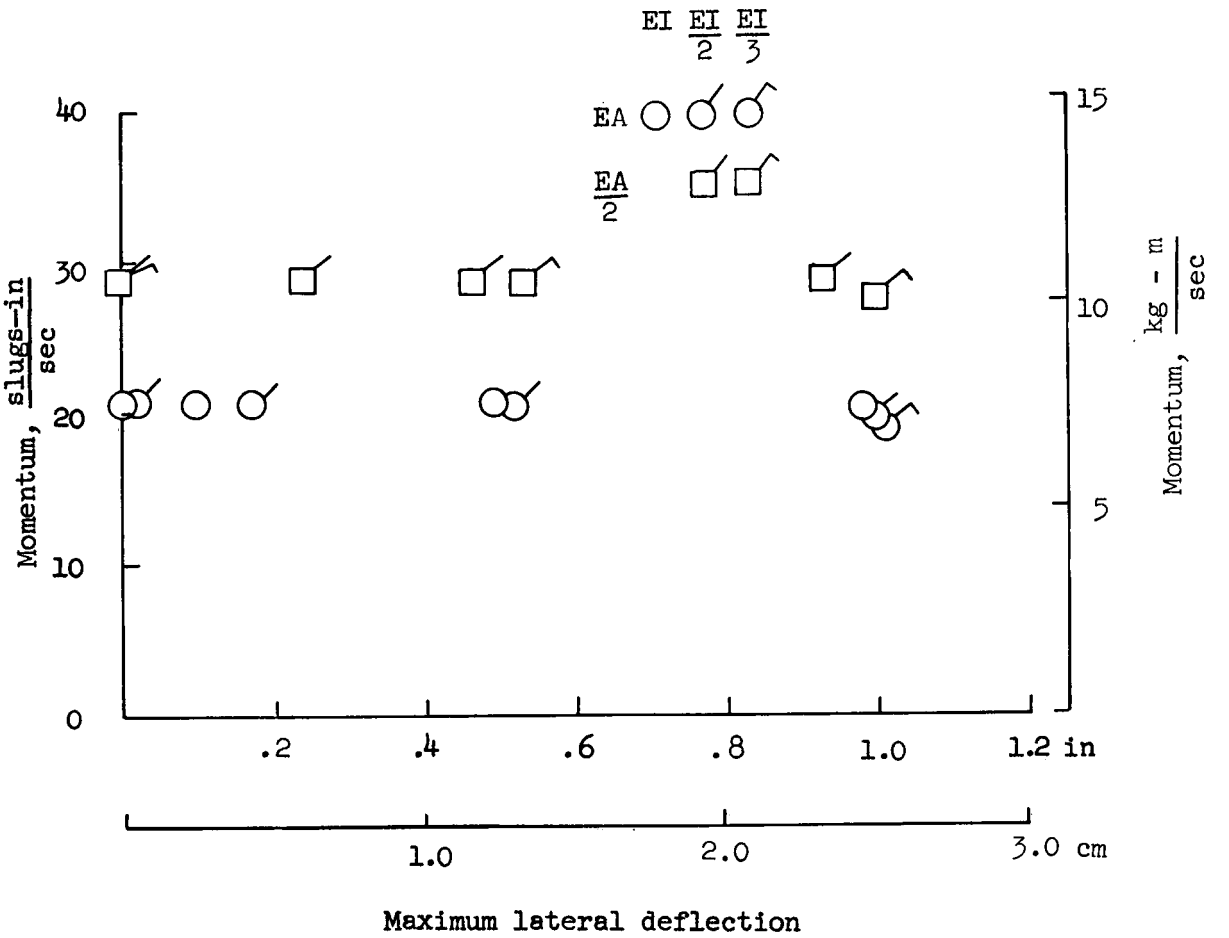

Figure 14.- Effect of longitudinal and lateral stiffness on maximum upward momentum of vertically impacting strut with shock absorber.

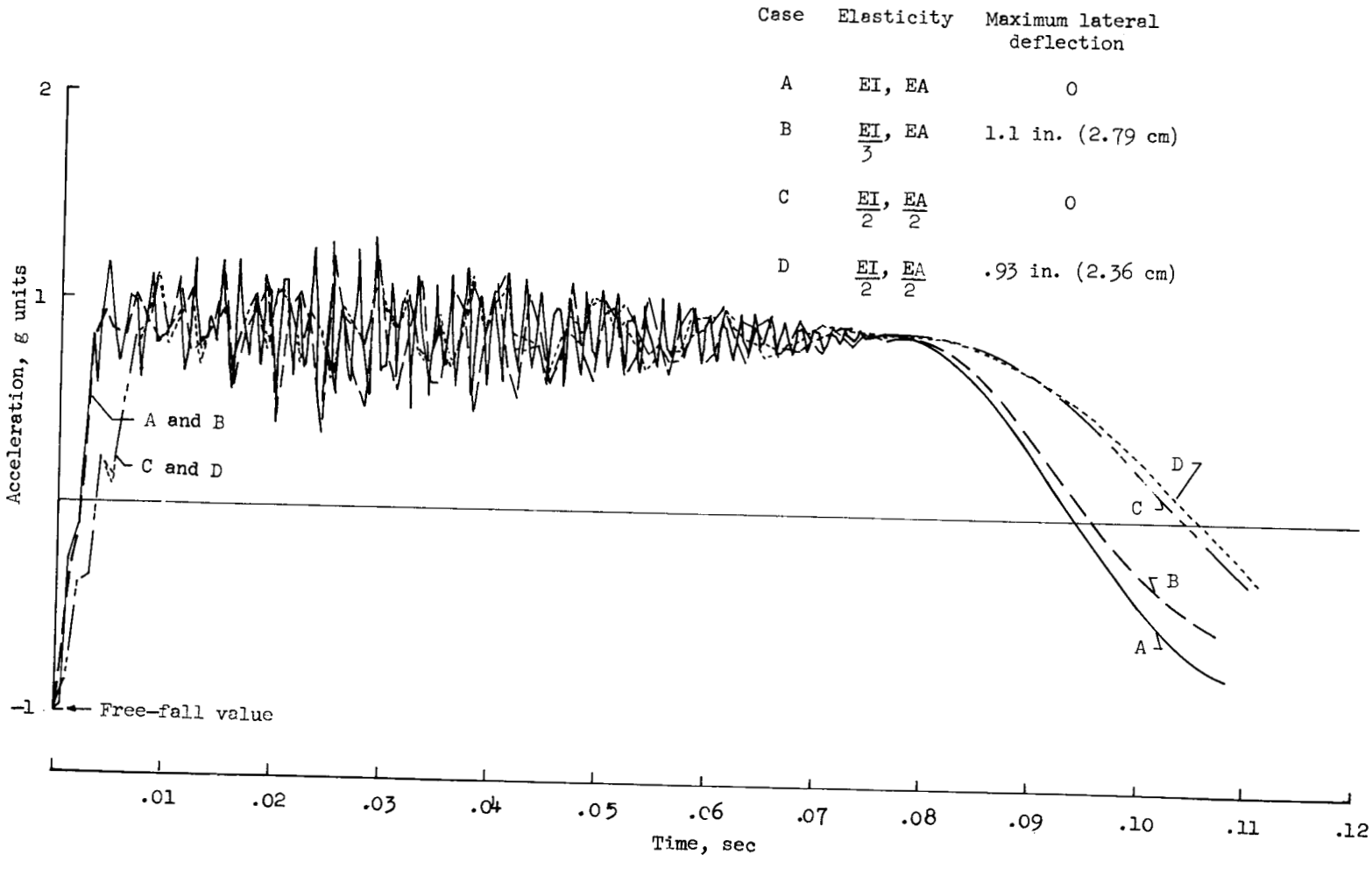

Figure 15.- Effect of stiffness on vertical-acceleration time history of upper mass of strut impacting at 2 ft/sec (0.6096 m/sec).

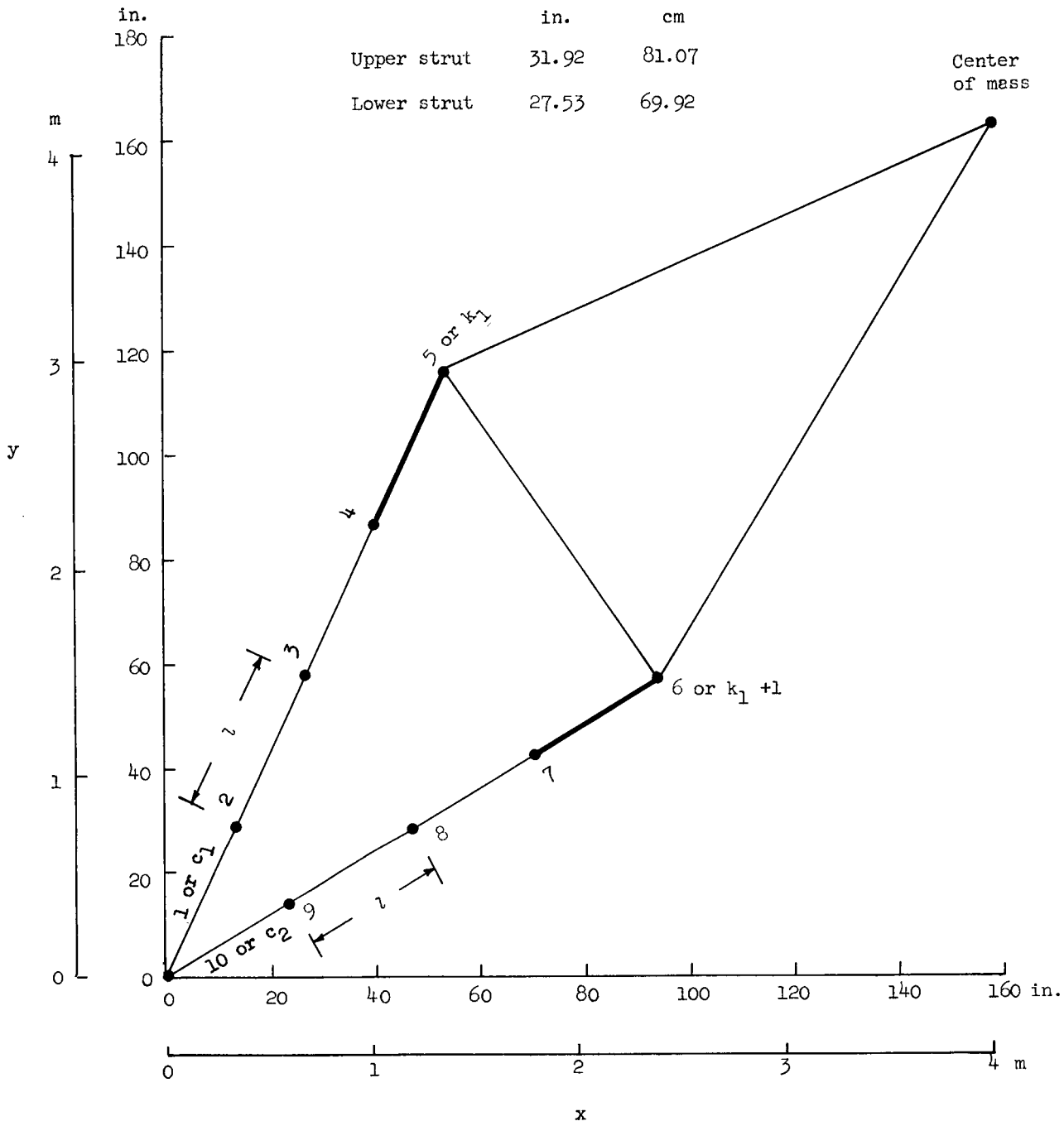

Figure 16.- Analytical model of a lunar-landing vehicle.

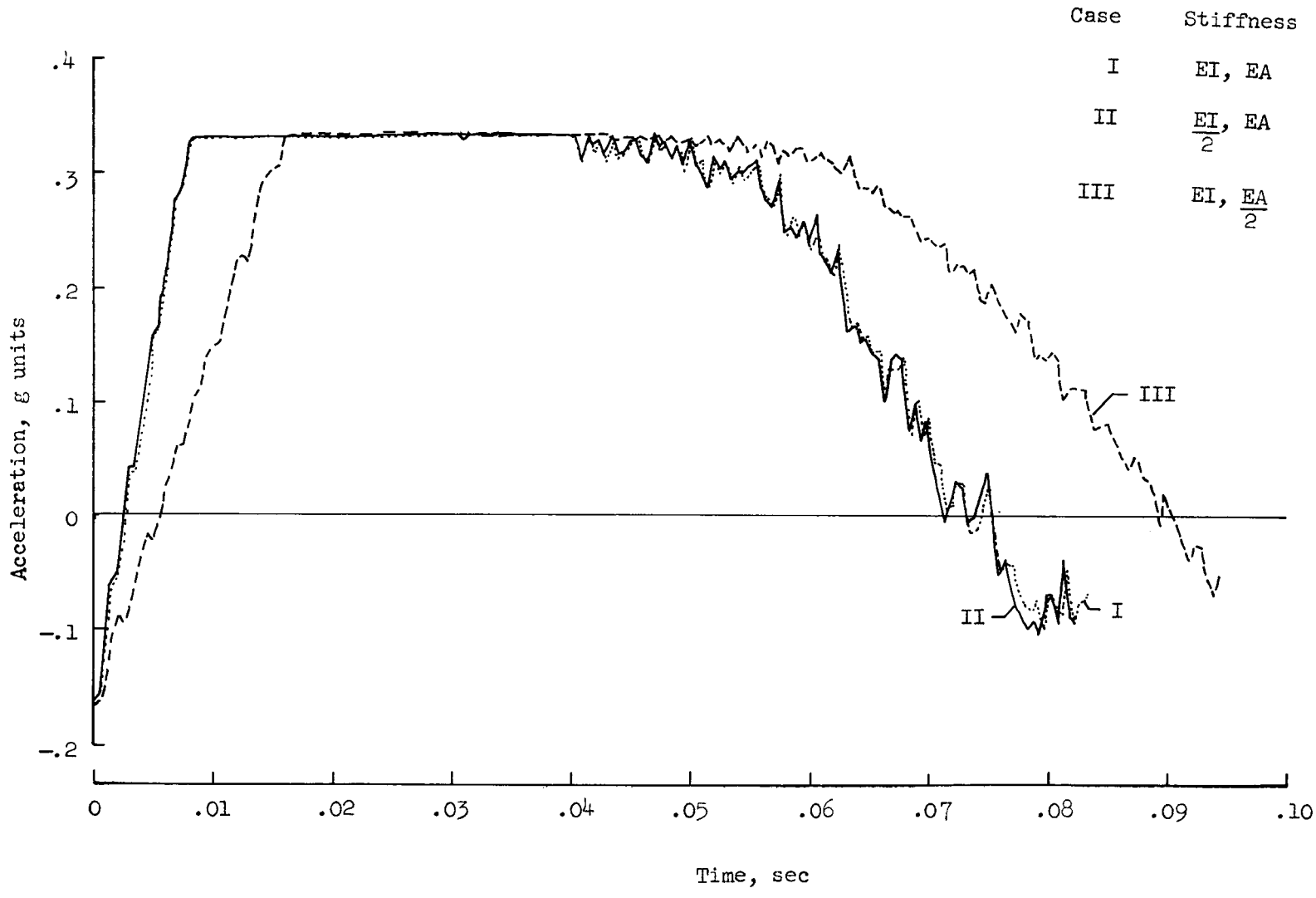

Figure 17.- Effect of landing-gear stiffness on vertical acceleration of center of gravity of lunar-landing vehicle impacting at 1 ft/sec (0.3048 m/sec).